Design, Development and Fabrication of Patch Compensated Wideband Vivaldi Antenna and Its Analysis in Radome Chamber

A Dissertation submitted towards the partial fulfilment of requirement for the award of degree of

MASTER OF ENGINEERING
IN
WIRELESS COMMUNICATION

Submitted by

Rajveer Dhawan
Roll No. 801463020

Under the guidance of

Dr. Vinay Kumar
Assistant Professor, ECED
Thapar University, Patiala

ELECTRONICS AND COMMUNICATION ENGINEERING DEPARTMENT
THAPAR UNIVERSITY
(Established under the section 3 of UGC Act, 1956)
PATIALA – 147004, PUNJAB, INDIA
JULY-2016

DECLARATION

I, **Rajveer Dhawan**, hereby declare that the dissertation entitled "**Design, Development and Fabrication of Patch Compensated Wideband Vivaldi Antenna and Its Analysis in Radome Chamber**" is an authentic record of my own work carried out for the award of degree of Master of Engineering in Wireless Communication from Thapar University, Patiala, under the supervision of **Dr. Vinay Kumar**, Assistant Professor, Electronics and Communication Engineering Department.

The matter presented in this dissertation has not been submitted in any other University/Institute for the award of any other degree.

Date: 14-07-16
Place: Patiala

Rajveer Dhawan
Roll no. 801463020

This is to certify that the above statement made by the student is correct to the best of my knowledge and belief.

Date: 14-07-16
Place: Patiala

Dr. Vinay Kumar
Assistant Professor
ECED, TU, Patiala

Countersigned by:

Dr. Sanjay Sharma
Professor and Head ECED
Thapar University, Patiala

Dr. S.S. Bhatia
Dean of Academic Affairs
Thapar University, Patiala

ACKNOWLEDGMENT

With deep sense of gratitude I express my sincere thanks to my esteemed and worthy supervisor, **Dr. Vinay Kumar,** Assistant Professor, Department of Electronics and Communication Engineering, Thapar University, Patiala for his valuable guidance in carrying out work under his effective supervision, encouragement, enlightenment and cooperation. Most of the novel ideas and solutions found in this dissertation are the result of our numerous stimulating discussions.

I shall be failing in my duties if I do not express my deep sense of gratitude towards **Dr. Sanjay Sharma,** Professor and Head, Electronics and Communication Engineering Department, for providing us with the adequate infrastructure for carrying out the work. I am also thankful to **Dr. Amit Kumar Kohli,** P.G. Coordinator, and **Dr. Hem Dutt Joshi,** Branch Coordinator, Electronics and Communication Engineering Department, for the motivation and inspiration that triggered me for the work.

I am also thankful to **Dr. Rana Pratap Yadav**, Assistant Professor for his kind and humble support at each and every step and **Dr. Rajesh Khanna**, for testing of antenna with VNA.

I am greatly indebted to all my friends who constantly encouraged me and also would like to thank the entire faculty and staff members of Electronics and Communication Engineering Department for their unyielding encouragement.

At last but not the least my gratitude towards my parents, who always supported me in doing the things my way and whose everlasting desires, selfless sacrifice, encouragement, affectionate blessings and help made it possible for me to complete my degree.

Place: TU, Patiala
Date: 14-07-16

Rajveer Dhawan
Roll No. 801463020

ABSTRACT

Design, development and fabrication of micro-stripline based Vivaldi Antenna for frequency range of 5.5-8.5 GHz has been presented. The Vivaldi antenna is a planner antenna, fabricated at micro-strip by having an exponentially tapered slot profile on it. A parametric study is done to clearly understand the antenna design and parametric variation effects on the radiation pattern. After that an optimized computer aided design has been developed and simulated where the results obtained are for the desired radiation parameters in terms of the VSWR, directionality, beam-width and bandwidth. The optimized design has been fabricated and tested. Wherever results are not found in agreement to simulation; problem has been comprehensively investigated and analysed. This is found associated with discontinuity at feed line, fabrication tolerance constraints and parasitic capacitance at edges or bent of micro-stripline which introduce the parasitic reactance in antenna design. A generalized theoretical procedure has been developed which explores that the associated problems can be compensated by incorporating inductive patch on feed line. The developed theory is applied in fabrication and effectively compensated the associated problems where test results are found in good agreement with simulation results. Further the Vivaldi antenna is studied in Radome enclosure for the operating frequency of 5 GHz. A computer aided design is developed in order to study the effect of Radome boundary on the radiation pattern and the performance characteristics of the Vivaldi Antenna. The design computes the VSWR, directionality, beamwidth and side lobes patterns that are being affected by using the Radome boundary. The overall design is simulated on COMSOL Multiphysics software.

Table of Contents

List of Figures

Chapter 8 Vivaldi Antenna enclosure in Radome Chamber

List of Tables

List of Acronyms

AVA	: Antipodal Vivaldi Antenna
BAVA	: Balanced Antipodal Vivaldi Antenna
CWSA	: Constant Width Slot Antenna
DSVA	: Double Slot Vivaldi Antenna
EM	: Electromagnetic Waves
FDTD	: Finite Difference Time Domain
FNBW	: First Null Beam Width
HPBW	: Half Power Beam width
LTSA	: Linearly Tapered Slot Antenna
PCB	: Printed Circuit Board
PEC	: Perfectly Matching Layer
PTFE	: Polytetrafluoroethylene Shell
PML	: Perfectly Matched Layer
RSE	: Regular Slot Edge
RF	: Radio Frequency
TSA	: Tapered Slot Antenna
TSE	: Tapered Slot Edge
UWB	: Ultra-Wide Band
VNA	: Vector Network Analyser
VSWR	: Voltage Standing Wave Ratio
ZIM	: Zero Index Materials

Chapter 1

Introduction to Basic Theory of Antenna

1.1 Antenna Definition

An antenna behaves like an electrical circuit in microwave/RF networks which enables the matching of the signal with the transmission line, which is either a coaxial cable or a waveguide. In nutshell, it can be said that antenna is somewhat similar to a transducer which converts electrical energy into an RF signal. Hence this electrical device works as an agent for transmitting or receiving electromagnetic signals.

1.2 Propagation Principles

In order to clearly understand the working principle of antenna, it is required to have knowledge of propagation principles, electromagnetism theory and Maxwell's equations. First, it is required to describe the signal which transmits through the cable, and then the signal propagation in free space and then a theory for the signal transformation. At the microscopic level, both the electric as well as the magnetic phenomena are explained by Maxwell's equations. Because of the electric current movement, signal travel in a cable which results in induction of electromagnetic field and this time-varying field generates em waves.

The major work of an antenna device is to control propagating em waves in order to get the radiation pattern in a certain frequency range, or in a particular direction, or desired power levels, or polarization. In order to achieve above stated objectives, a number of different types and design of antennae with different functions and practical solutions are introduced. But, still the crucial part is to attain desired current distributions over the geometry of antenna.

1.3 Classification of Antennas

Antennas can be categorized in various ways, adhering to the design principles, radiation pattern, operating frequency band or according to the field of use and application. On the basis of physical structure antenna can be categorized into following classes:

1. Wire antennas (dipoles and loops)
2. Aperture antennas (pyramidal horns)
3. Reflector antennas (parabolic dish antennas)
4. Microstrip antennas (patches)
5. Dielectric antennas (dielectric resonant antennas)
6. Active integrated antennas
7. Lens antennas (sphere)
8. Leaky wave antennas.
9. Antenna arrays (including smart antennas)

Also, antennae can also be categorized on the basis of operating frequency band i.e. a narrowband, wideband or ultra-wideband. Adhering to the radiation pattern antennae can be categorized as end-fire or broadside, omnidirectional or single or multiple directed antennae.

In accordance to the work in report, the Vivaldi antenna belongs to a class of ultra-wideband microstrip antennae.

1.4 Basic Parameters of Antennas

For describing the antenna's performance, various defining parameters [1] need to be discussed first. These parameters are quoted from the *IEEE Standard Definitions of Terms for Antennas*.

1.4.1 Radiation Pattern

It basically defines the radiation behavior of antenna with respect to space coordinates. The radiation pattern is defined in its polar coordinates which are calculated at far field. Power flux density, radiation intensity, directivity, field strength and polarization are some of the properties that can be evaluated by studying radiation pattern. Field Pattern is generally described as a linear scale plot that evaluates the amplitude of either magnetic or electric field in angular space whereas Power Pattern (Linear Scale) evaluates the squared value of magnitude of either magnetic or electric field in angular space.

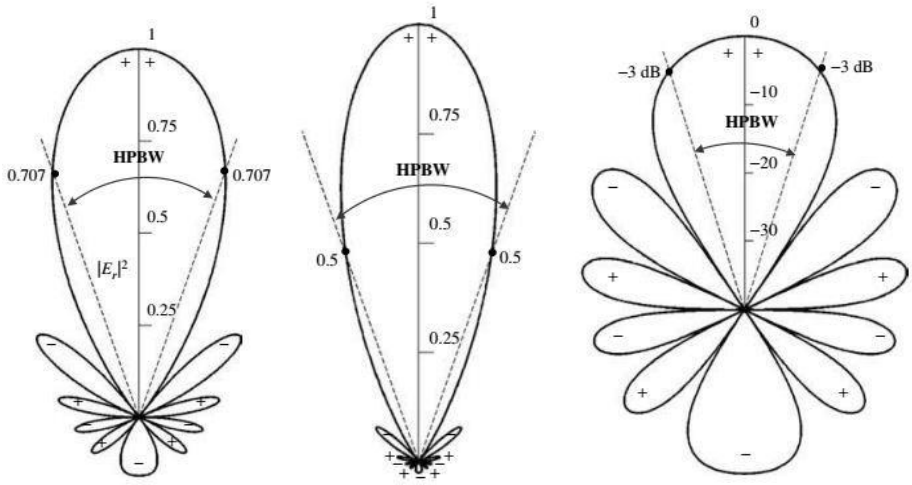

Fig.1.1 (a) Field pattern described in linear scale

(b) Power pattern described in linear scale

(c) Power pattern described in dB.

Power Pattern (logarithmic scale dB) evaluates either the magnetic or electric field in decibels, as a multinomial of angular space.

1.4.2 Field Regions

The space encompassing an antenna is sub-categorized mainly into three regions:

(a) Reactive Near-Field

(b) Radiating Near-Field (Fresnel)

(c) Far-Field (Fraunhofer)

The space just after the boundary of antenna is defined as *Reactive near-field region*. This region exists for a distance of $R < 0.62\sqrt{D^3/\lambda}$ where λ is the wavelength and D is dimension of antenna.

Radiating near-field (Fresnel) region is defined as "The space wherein the radiation field is mostly dominated and where the angular field distribution is a function of the distance from the antenna. This region exists at$0.62\sqrt{D^3/\lambda} \leq R < 2\,D^2/\lambda$.

The space where the angular field distribution is independent of the distance from the antenna is termed to be *Far-field (Fraunhofer) region*. This region extends for $R \geq 2\,D^2/\lambda$.

1.4.3 Radiation Pattern Lobes

Diverse forms of radiation pattern are mentioned as lobes, which can be further categorized as major, minor, side and back lobes. A radiation lobe, is a chunk of radiation pattern allied with relatively weak radiation intensity. The radiation lobe encompassing the orientation in direction of maximum radiation is said to be Major Lobe. All other lobes except the major lobe is said to be Minor Lobe. The lobe whose axis is exactly opposite to the major lobe is termed as Back Lobe.

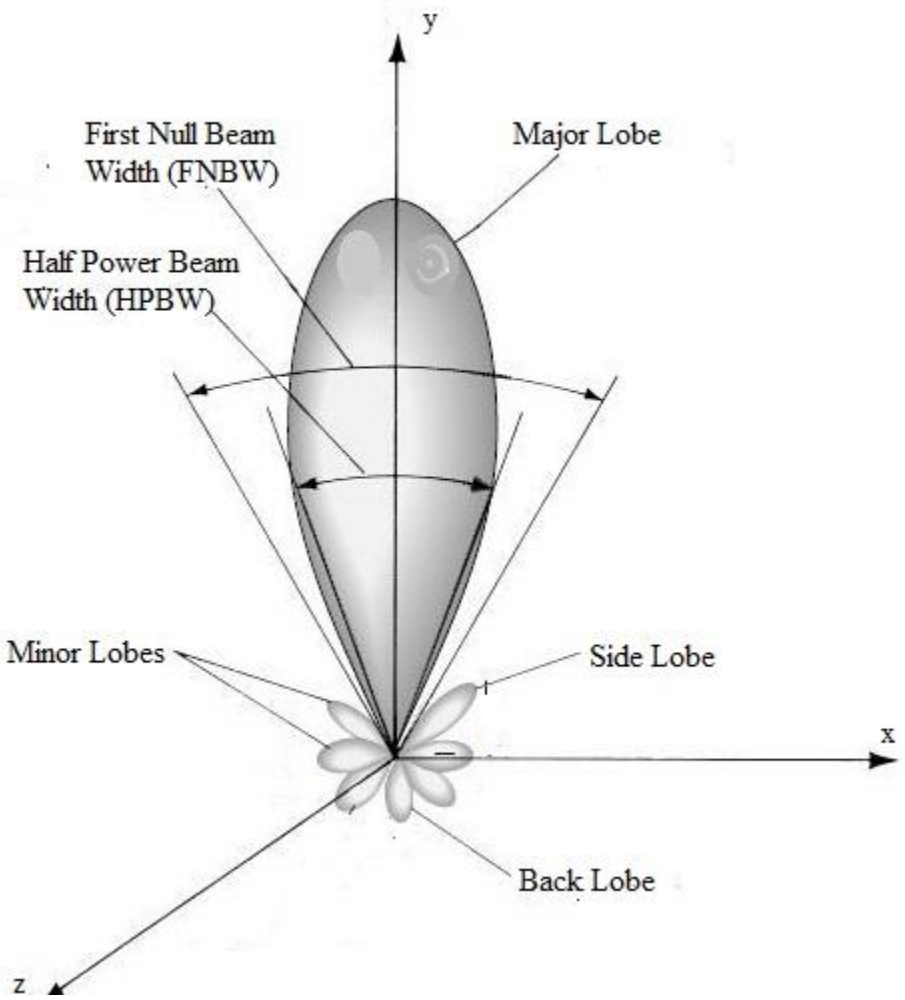

Fig.1.2 Radiation lobes and beamwidth of an antenna pattern.

1.4.4 Beamwidth

The beamwidth of radiation pattern can be determined by evaluating the angular separation between two homogeneous points in the major lobe. Basically beamwidth is categorized as HPBW and FNBW. The angular separation at which the radiation intensity is one half of the major beam is stated as HPBW whereas the angular separation between the first nulls is stated as FNBW as shown in Fig. 1.2

1.4.5 Radiation Intensity

Radiation intensity is termed as the power emitted by an antenna in a specified direction per unit solid angle. It is a far-field parameter which can be evaluated by the product of radiation density with the square of the distance. It can be expressed mathematically as

$$U = r^2 W_{rad}. \tag{1.1}$$

1.4.6 Directivity

Directivity is a dimension less quantity and can be defined as the total radiation intensity in a specific direction divided by the radiation intensity averaged over all directions. The average radiation intensity can be evaluated by dividing total power radiated by 4π.

$$D = 4\pi U / P\_rad. \tag{1.2}$$

1.4.7Gain

Gain of an antenna is defined as the ratio of the radiation intensity, in a particular direction, to the radiation intensity which can be obtained if the power accepted is radiated isotropically.

$$G = 4\pi U / P\_in. \tag{1.3}$$

1.4.8 Antenna Efficiency

Antenna efficiency is the ratio of gain to directivity.

$$\eta = G/D. \tag{1.4}$$

1.4.9 Polarization

Polarization is a parameter which is used to study the time varying directive nature of electric or magnetic field vector. It can be subcategorized as linear, circular and elliptical.

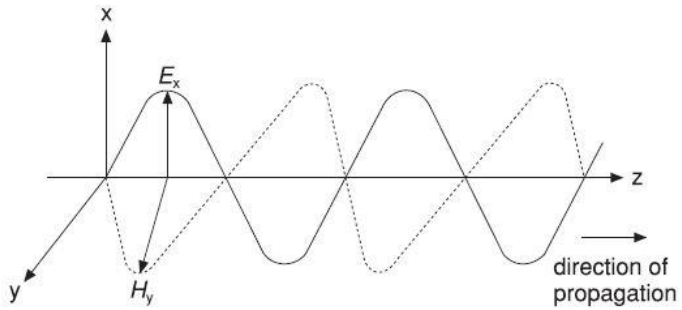

Fig.1.3 Diagram shows orientation of E and H component for an em wave.

If the electric or magnetic field vector always point to a specific direction or line then the behavior is termed as linear polarization. Similarly if the electric or magnetic field vector traces the pattern of a circle then this behavior is said to be circularly polarized whereas if the pattern is elliptical in nature then it is said to be elliptically polarized.

1.5 Microstrip Transmission Line

Microstrip is an electrical transmission line. It is implemented on printed circuit board and used to transmit em signals. Microstrip comprises of conducting strip on a ground plane.

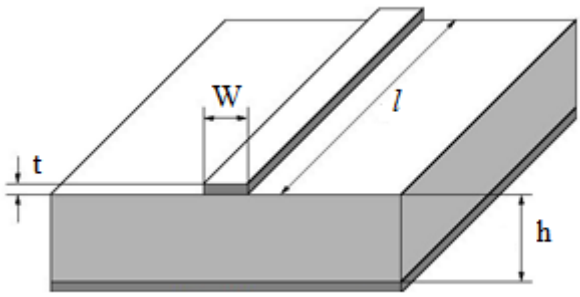

Fig.1.4 Block diagram shows a schematic prototype
for designing a microstrip feedline.

The impedance of the transmission line depends on the dimension of the microstrip line which is guided by the following equations [2]:

For $W/h \leq 1$, $$Z_0 = \frac{60}{\sqrt{\varepsilon_e}} \ln\left(\frac{8h}{W} + \frac{W}{4h}\right). \quad (1.5)$$

For $W/h \geq 1$, $$Z_0 = \frac{120\pi}{\sqrt{\varepsilon_e}\left[\frac{W}{h} + 1.393 + 0.667 \ln\left(\frac{W}{h} + 1.444\right)\right]}. \quad (1.6)$$

If it is required to evaluate the dimensions of transmission line for a particular impedance value than following equations can be taken into account:

$W/h < 2$, $$W = h\frac{8e^A}{e^{2A} - 2}. \quad (1.7)$$

$W/h > 2$, $$W = \frac{2h}{\pi}\left[B - 1 - \ln(2B - 1) + \frac{\varepsilon_r - 1}{2\varepsilon_r}\left\{\ln(B - 1) + 0.39 - \frac{0.61}{\varepsilon_r}\right\}\right]. \quad (1.8)$$

Where $$A = \frac{Z_0}{60}\sqrt{\frac{\varepsilon_r + 1}{2}} + \frac{\varepsilon_r - 1}{\varepsilon_r + 1}\left(0.23 + \frac{0.11}{\varepsilon_r}\right). \quad \text{and} \quad B = \frac{377\pi}{2Z_0\sqrt{\varepsilon_r}}. \quad (1.9)$$

The effective dielectric value'ε_e' varies according to the design parameters of microstrip i.e. the height 'h' of the substrate and the width 'W' of the transmission line which can be clearly explained by following equation:

$\varepsilon_e = \frac{\epsilon_r + 1}{2} + \frac{\epsilon_r - 1}{2}\left(\frac{1}{\sqrt{1 + 12h/W}}\right)$. where ε_r is the dielectric constant value of conduct strip.

Chapter 2

Literature Survey

Yngvesson et al. [5] compared three different TSAs i.e. linear TSA, fixed width TSA and exponential TSA. The results show that maximum number of side lobes are obtained in LTSA followed by FWSA and Vivaldi antenna whereas Vivaldi has the widest beamwidth followed by LTSA and FWSA. The report also shows the effect of thickness of the dielectric substrate. The increase in thickness of dielectric substrate results in increased gain along with increase in higher number of side-lobes.

Gazit et al. [6] employed two major changes to the conventional Vivaldi design i.e. insertion of an antipodal slotline with a relatively lower dielectric substrate cuclad instead of alumina. An antipodal transition is designed by taking the tapered microstrip line via a parallel strip along both the sides of the slot line. This type of mechanism offers a wide band-width in comparison to which is obtained by the traditional design. However, with the fusion of antipodal slotline transition there arises a problem of mismatch in polarization resulting in cross polarization.

Kollberg et al. [7] in order to introduce a handy fabrication, used circular stubs to provide microstrip to slotline transition. A model of network description for transmission-line is given to analyze the feedline design. Different type of transitions i.e. transitions with uniform and non-uniform lines are soldered and are treated as virtually shorted microstrip lines. The soldered microstrip transition offers the widest bandwidth. Optimal combinations can be found by modelling different microstrip and slot stub diameters. Virtual short via circular microstrip stub provides 10% lower bandwidth in comparison to the maximum value for the soldered one. The modelling results are experimentally verified by evaluating the transmission coefficient for two cascade transitions separated apart by a slotline within 1-16 GHz frequency range.

Langley et al. [8] incorporated some modifications in the antipodal design transition by assimilating an improvised and balanced structure that provided relatively small level of cross polarization. The proposed structure, defined as balanced antipodal arrangement, comprises of three tapered slot layers which are directly fed by a stripline.

The introduction of defined layer results in balancing of Electric-field behavior in antipodal transition. The taper slot work as ground plane on both sides of the substrate. This transition provides relatively better cross polarization characteristics.

Hall et al. [9] designed a wide bandwidth phased array. This structure incorporated microwave integrated circuit which is used as a stripline to microstrip transition, dielectric constant equal to 10.5, and a loss of less than 10dB. Asymmetrical flares are used to control the radiation pattern whereas a squint in E-plane is noted. By incorporating semicircular substrate extension, mismatch at flare aperture is reduced and performance can be altered by affecting the dielectric air interface at the flared end.

Sloan et al. [10] introduced radial stubs instead of using circular that resulted in improved bandwidth for these type of transitions. A dual slot-line transition provides a 90° cross in comparison to the circular one. Radial stubs at the transmission line provide 1.3 dB of insertion loss which was comparatively less than that was measured (0.65 dB per transition) at 3–15 GHz. The entire structure of transition is simulated on an electromagnetic finite-element simulator.

Shin et al. [11] employed both stubs i.e. circular and radial. A stripline-fed is designed by using metal fins on both sides of the element. In particular, it is found that these non-uniform stubs result in the improvement of bandwidth whereas the radial stub found to be more beneficial in comparison to circular stub. The results also prove that the use of stripline feeding increases the antenna bandwidth as compared to the microstrip feeding.

Chio et al. [12] defined the fundamental parameters which affect the bandwidth and wide-scan performance of the antenna. The performance improves at the lower end of operating frequency band in H plane. The mid-band performance is determined by the rate of the taper slotline. In order to achieve balanced performance in the mid-band, opening rate is to be chosen wisely. In the lower frequency band, longer taper slotline results in increase of bandwidth of the antenna. A comprehensive parametric study of TSA is done by full-wave MoM technique. Parametric analyzation is done for each design parameter where obtained results are compared in terms of SWR and antenna gain plot.

Kim et al. [13] studied previous design of antipodal Vivaldi antenna which provided relatively good performance but with an unfortunately high level of cross-polarization that incurred due to the flares on the substrate. The concept of placing antipodal antenna with its mirror image in H plane is used in order to reduce the cross-polarization level. This type of mechanism results in 20 dB reduction in cross-polarization at broadside.

Dotto et al. [14] designed a 3-D structure which was nearly a type of fleur-de-lis. This proposed structure of new balanced antenna is unique which provides an extremely flat S_{11} response with low phase distortion in a frequency band of 2.2-21 GHz. The S_{11} response of antenna developed at the LEAT in comparison to conventional Vivaldi antenna results in much better performance.

Tianming et al. [15] introduced antipodal Vivaldi antenna for the application of pulse radiation in UWB communication. The proposed design of UWB antenna which is assigned to wireless communication shows good performance in terms of little distortion, good directivity and high efficiency over a frequency range of 3.1GHz to 10.6GHz.

Cerny et al. [16] proposed a design for minimizing the back radiations of Vivaldi antenna in order to use it for radar application. Several design techniques are incorporated like shielding of the back or skewed boxed antenna with planar back-plane in order to minimize back radiations. The back radiation results in reflection from the radar operator, which shows a negative influence on the captured signal. Thus, there is a distortion in the measured view of the guarded area or the unwanted reflections lead to a wrong alarm. Hence, above stated techniques are introduced in design in order to minimize the reflections.

Deng et al. [17] designed 2-dimension structure of Vivaldi antenna with a low profile and compared it with UWB antennas. The conventional Vivaldi design has a large-size with limited bandwidth constraints. The key factors responsible for limiting the bandwidth of antenna are analyzed and minimized by introducing a chip resistor and short pin in the conventional design. An antenna design is fabricated for 1–20 GHz whereas the measurement results in 0.9 dB of gain at 1 GHz and the VSWR is better than 2.0 for whole of the band.

Artiga et al. [18] presented a Vivaldi antenna having the ability of rejecting interferers with dynamic frequencies allocation besides aiming at multi-standard communication. Half element of Vivaldi is used for operation which is placed over a ground plane. This type of geometry is suitable for vehicular communication. The rejection filter which comprises of two microstrip resonators along with varactor diodes which are coupled with the slot of the Vivaldi, is incorporated in the antenna design. Controlled voltage at the antenna RF port is used for biasing of the design. The modified design provides a good matching for 2.5 to 8 GHz frequency band along with 20 dB gain rejection in the direction of maximum radiation.

Kim et al. [19] introduced beam correction technique for Vivaldi antenna with shorting pin in the structure. The design is fed on a taper section by a microstrip transmission line. The asymmetric current distribution results in tilting of the main beam which is corrected by using shorting pin at the edge of the side arm. The incorporation of shorting pin structure results in improved radiation pattern along with wideband operation characteristic.

Lizhong et al. [20] proposed a design to implement the practical work for fabrication of dual polarized (UWB) Vivaldi at a frequency range of 3.1-10.6 GHz. The design comprises of two orthogonal single polarized Vivaldi antennas where a linear taper feeding structure is used to realize the impedance matching. Two independent separate feeding structures are incorporated in dual polarized Vivaldi antenna design. The fabricated design is tested in anechoic chamber which results in 1.37dBi gain for each polarization port and shows an isolation degree of about 20dB. The performances of both the ports are not symmetric and other performance parameters are not in good association with the simulation results. This should be further enhanced by removing the fabrication constraints.

Zhou et al. [21] used a layer of anisotropic zero-index metamaterials (ZIM) which is coated on the end of exponential slot in order to enhance the bandwidth as well as the directivity of the Vivaldi antenna. Anisotropic ZIM are fabricated in the design by using resonant meander-line structures. Tested results show an increase in the main lobe gain as well as the directivity of the Vivaldi antenna in a frequency band of 9.5–10.5 GHz.

Yang et al. [22] improved the design of Vivaldi antenna by incorporating a current chocked structure. The design is simulated at a frequency range of 0.5 to 3 GHz which results in relatively low cut-off frequency and high frequency gain in comparison to conventional design. The current choke structure is designed by introducing a set of rectangular gratings which are etched on the Vivaldi antenna prototype. FDTD method is used to optimize the current choke elements in the design. The improved design offers about 3.1dB higher gain at low end of operating frequency with reduction in cut-off frequency.

Wang et al. [23] enhanced the performance parameters like the gain and directivity of antenna. A double-slot structure is proposed in which both the slots are uniformly excited by using a power divider T-junction. The double-slot mechanism generates plane waves along the taper slot of the antenna which results in significant increase in the gain as well as more directional behavior of the DSVA. The double-slot Vivaldi performs well in 2.5–15 GHz of frequency band and the E-field peak gain is much higher in comparison to that of the conventional Vivaldi antenna from 6 to 15 GHz.

Xinyu et al. [24] proposed antenna design using Vivaldi construction and theory technique for THz band. The design is optimized and simulated using 3-D finite-integral time-domain technique for a band of 155-180 GHz. The antenna design adopts polyethylene medium for reducing Power Loss and introduces choke groove in design for restraining back flow and reflection. Further directionality is enhanced by using array technique, hence the proposed design structure provides application in modern THz communication systems.

Shan et al. [25] improved the directivity of the antenna in order to design it for vehicular and wireless local area networks applications. On the front end of the aperture planar directors are incorporated on the tapered and transverse slots of the antenna. The results show an increase by 1.5 dB of gain in comparison to normal one for IEEE 802.11a (5150-5935 MHz) WLAN. The proposed design also shows high directivity for 2400-2483 MHz and 3560-3700 MHz band, IEEE 802.11b IEEE 802.11y respectively for WLAN, or other wireless communication systems. Further, the modified design of Vivaldi antenna provides low polarization distortion which incurred due to the roof of car, thereby behaving as a large ground plane in comparison to the conventional one.

Liu et al. [26] introduced a new stepped connection structure between tapered patches and slotline and adopted the above stated modifications in a planar printed Vivaldi antenna. The stepped connection structure provides a significant improvement in impedance matching along with wide bandwidth. A prototype of the modified design of Vivaldi antenna is fabricated in order to explain the effectiveness of this design. Tested results reveals that there is a significant improvement of impedance matching in frequency band of 3 to 15.1 GHz, further the measured gain is better than 5 dBi along-with enlargement of bandwidth without affecting previous design dimensions. Besides, a flat time delay response is noticed in the band of 3–15.1 GHz.

Sonkki et al. [27] presented a dual-polarized, wideband Vivaldi antenna with over a decade (10.7:1) of bandwidth. Two orthogonal Vivaldi antennas are placed in a cross-shaped form in order to achieve a dual-polarized antenna structure, without a galvanic contact. This design provides a loss of nearly10 dB over a frequency of 0.7 -7.30 GHz. The isolation (S21) is observed to be better than 30 dB between the antenna ports, and a maximum gain of 3.8–11.2 dB is seen at the aforementioned frequency bandwidth. The cross-polarization discrimination (XPD) is found to be better than 25 dB up to 4.5 GHz, and better than 19 dB over 0.7–6.0 GHz frequency bandwidth. The tested results are compared in terms of XPD, maximum gain and S-parameters.

Weller et al. [28] introduced a novel method for boosting the bandwidth and directivity of the antipodal Vivaldi antenna. The technique is based on incorporating an elliptical parasitic patch at the flared end in order to raise the field coupling between the arms which is used to produce strong radiations towards the endfire direction. This approach refines the directivity without affecting the low frequency performance and it also eliminates the need of electrically thin dielectric substrates. The proposed antenna structure has a peak gain >0 dBi for a frequency band of 2–32 GHz and >10 dBi over 6–21 GHz frequency band, which confirms as an improvement over conventional designs that has been reported for Vivaldi antennas with similar size.

Perotoni et al. [29] proposed an improved radiative featured design for exponential slotted-edge Antipodal Vivaldi Antenna, as compared to the conventional AVA design. The design improves squint effect with low-end bandwidth limitation and reduces both the side and back lobe level and also enhances the main lobe gain. In order to justify the features, a comparative study is done on two types of slot in the design i.e. regular

slot edge (RSE) and the tapered slot edge (TSE) in AVA. The comparison shows an improved gain of 8.3 dB at 6 GHz whereas a loss of 15.5 dB in Side Lobe Level with 0 degrees shift in main lobe squint. Comparing the different types of slot i.e. the ESE-AVA with RSE-AVA and TSE-AVA, it is observed that the notches are similar to the main radiator, which mitigates the SLL besides directing E-fields distributions along the main lobe.

Dastranj [30] proposed a modified broadband AVA for a frequency band of 6–18 GHz. The design introduces round corners for the patches, in order to mitigate the diffractions from sharp ends. This modification results in the gain as well as the directivity improvement of the antenna. Besides, one major change is made on the background plane of the antenna design which fulfills the purpose of reflecting radiation from the backplane in a direction that is opposite to the required direction. This incorporation effectively increase the radiation in forward direction, thus results in 7–8.4 dB gain along-with stable radiation pattern with the designed low cross-polarization. The modified design is fabricated and verified experimentally, where the results are in reasonable agreement with the simulation data.

Kharkovsky et al. [31] presented an improved compact design of antipodal Vivaldi antenna having good performance over various applications of microwave as well as millimeter wave imaging. Periodic slit edges are cut in the design of AVA which behaves as a trapezoid-shaped dielectric lens. This structure enhances the performances in terms of wide bandwidth, high gain, low front-to-back ratio and more directional behavior with modification in E-plane beam tilt, along with small side-lobe levels. Incorporation of periodic slit edge on the outer boundary of the antenna radiators results in providing low-end limitation without modifying the dimensions of the antenna. This optimized design of antenna is fabricated and tested where the results show S_{11}< -10 dB for a frequency band of 3.4 to 40 GHz, which are also in good agreement with simulation results. The periodic slit edge elevates the gain up to 8 dB, whereas the trapezoid dielectric lens improves the gain up to 15 dB at lower and higher frequencies, respectively. The incorporation of the lens also improves the E-plane beam tilts and lowers side-lobe levels in the radiation pattern.

Qiu et al. [32] presented a compact circularly polarized antenna design by utilizing Vivaldi antenna structure. The antenna design comprises of four exponentially tapered

patches on a circular metal wall along-with a feed network. These four patches are rotated sequentially and placed vertically along the circular metal wall which behaves as a vertical ground plane. Slot-coupled feeding technique is applied which results in a wide impedance bandwidth. A parametric study is done in order to optimize the antenna where the experimental results exhibits a 10-dB impedance bandwidth of 57.3% (3.06–5.52 GHz) as well as a 3-dB AR bandwidth of 41.4% (3.45–5.25 GHz).

McEvoy et al. [33] designed an UWB solar Vivaldi antenna which fulfills the need for lossy power management by integrating amorphous silicon cells in antenna design that provides a peak power at 4.25 V. This device is capable of yielding solar energy as a function for harvesting dual-source energy. The solar Vivaldi provides a gain of nearly 0.5–2.8 dBi in a frequency band of 0.95–2.45 GHz.

Chapter 3

Gaps Analysis, Objective and Methodology

3.1 Gaps in Study

- Introduction of cross polarization while changing the antenna design.
- Impedance mismatching between antenna and RF source in fabrication.
- Shifting of main beam while implementing the design on PCB.

3.2 Objective

1. To find the reason for the ambiguities between the results of the simulation and fabricated design.
2. To purpose and study numerically, a theoratical procedure that can be applied to the antenna design in fabrication in order to get the desired results.
3. To analyse the radiation characteristics of the proposed design in radome chamber.

3.3 Methodology

The steps to design **"Design, development and fabrication of patch compensated wideband Vivaldi antenna"** and to characterize the outputs are as follows:

i. Study of COMSOL Multiphysics.
ii. Parametric study of Vivaldi antenna designing parameters.
iii. Simulation of the optimized design and compare the results with the fabricated antenna design.
iv. Analysis of the problems which occur due to discontinuity at feed line, fabrication tolerance constraints and parasitic capacitance at edges or bent of micro-stripline.
v. Numerical study of the compensation technique and applied in fabrication.
vi. Computer aided analysis of the design in radome chamber.

CHAPTER 4

Brief overview of Vivaldi Antenna

4.1 Introduction

The design of the antenna was first discussed by Gibson [4] in 1979.The Vivaldi antenna is a special kind of aperiodic travelling wave antenna. Here two words are mentioned to explain the behavior of Vivaldi antenna i.e. aperiodic and travelling. Aperiodic word emphasizes that the slot used in the design is aperiodic in nature whereas traveling emphasizes that the em wave will travel into the slot before leaving the antenna structure. Hence the design comprises of an exponential slot whose guiding equation for the curve can be expressed as

$$y = \pm c_1 e^{Rx} + c_2 \tag{4.1}$$

Where, R is the exponential factor. The beamwidth of the Vivaldi antenna is affected by this power factor whereas c_1 and $c_2$are constants. The design proposed by Vivaldi shows a significant improvement in antenna's performance parameters such as efficiency, gain, bandwidth and directivity.

4.2 What's in a Name?

Mr. Antonio Vivaldi introduced a musical instrument. On seeing the structure of that instrument Gibson got an idea for his antenna design. He was so much influenced by the structure of the musical instrument that he gave the name of the introducer to his antenna design.

4.3 Tapered Slot Antennas (TSA)

A TSA is a class of antenna having a feed line followed by an opening slot. The varying behavior of slot specifies various types of antenna. These profiles of TSA are generally specified as linear slot, constant width slot and exponentially tapered slot Vivaldi as shown below in Fig.4.1.

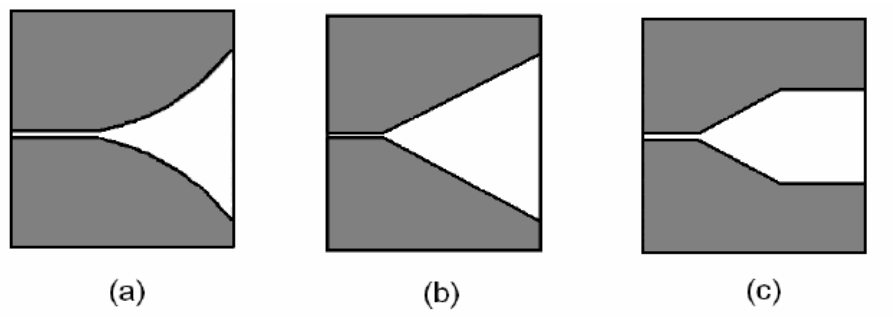

Fig.4.1 Types of TSA; (a) exponential tapered Vivaldi,
(b) linearly tapered (LTSA) and (c) constant width slot antenna (CWSA) [5].

4.4 The Principle of Operation

For briefly understanding the operating principle of Vivaldi Antenna, it is required to sub-divide the antenna design into two sections:

i. **Propagating section:** This section deals with the propagation of em wave from the feed line to the slot of the antenna. The portion in red depicts the em wave travelling from the microstrip feedline to the exponential feedline.
ii. **Radiating section:** This is the outermost section of slotline after which the em wave leaves the structure of the antenna.

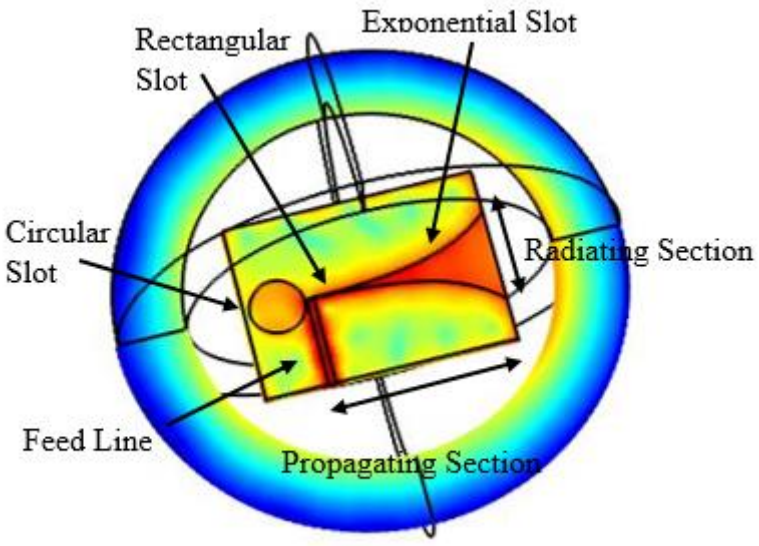

Fig.4.2. Layout of Vivaldi Antenna.

4.5 Basic structure of VIVALDI

From the above figure it can be seen that the Vivaldi antenna structure comprises of mainly three different type of slots i.e.

i. **The circular slot:** This slot provides the ability to tune the impedance of the antenna in order to perfectly match it with the impedance of the microstrip transmission line.
ii. **The rectangular slot:** This slot fulfils the purpose of coupling of em wave from the microstrip feed line to slot line.
iii. **The exponential tapered slot:** This slot provides the guiding path for the radiating em wave. The exponential rate of the curve is the determining parameter for the bandwidth and directivity of the radiation pattern.

An endfire radiation pattern is visualized and the electronic field is in the same plane of the dielectric substrate. The radiation pattern is linearly polarized in two planes, yet an elliptical polarization exists between the E plane and the H plane. The E plane and the H plane shows almost the same beamwidth and the cross polarization level is also low for it.

4.6 Advantages of Vivaldi Antenna

i. Configuration simplicity.
ii. Wide bandwidth.
iii. High gain at microwave frequencies.
iv. Broadband characteristics (suitable for ultra-wideband signals).
v. Easy manufacturing process using common methods for PCB production.
vi. Easy impedance matching.
vii. Low fabrication cost.

4.7 Geometry of Vivaldi Antenna

Some of the designing parameters are explained below which plays a major role in determining the antenna performance characteristics.

4.7.1 Substrate

Dielectric constant and thickness are the two major parameters which should be kept in mind while choosing the substrate of antenna.

- **Dielectric constant:** There is a trade-off condition while deciding the value of dielectric constant. Higher dielectric constant will result in shrinking of the dimension of antenna whereas substrate having a lower dielectric value will result in providing wider bandwidth.

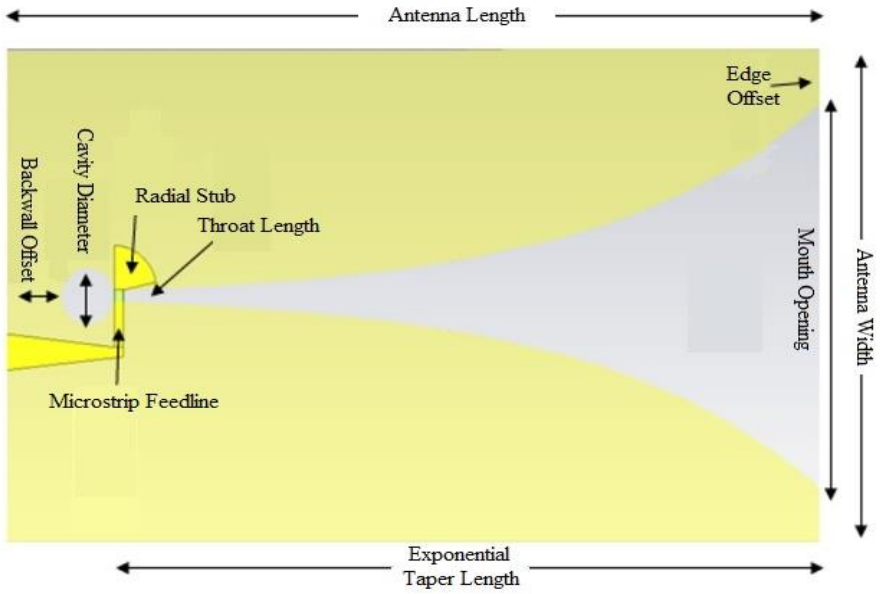

Fig.4.3 Vivaldi Antenna Structure.

- **Thickness:** The other important parameter related with substrate designing is its thickness. Increasing the thickness of the substrate results in improving the gain as well as the main beamwidth. The main reason behind this action is that the antenna impedance decreases as capacitance is inversely proportional to the distance between plates. During designing of antenna a FR4 substrate having relative permittivity 4.3 is taken whose thickness is 1.6mm and having 35µm copper layer on both sides. The substrate used here is the most preferable PCB board, which is cheap in cost and can be easily fabricated.

4.7.2 Antenna Length

There is a limiting condition on the length of antenna i.e. the antenna length should be greater than the average value of the maximum and minimum operating frequency [4, 12]. The bandwidth of antenna can be improved by taking a longer length.

$F_{\_max}$ *=6GHz; Fmin =2 GHz;* $\lambda = \frac{c}{f}$ *;* λmin *=50mm;* λ_max *=150mm;*

$L > \frac{\lambda min + \lambda max.}{2} = \frac{50+150.}{2} = 100mm$ *; So L is taken 110 mm.*

4.7.3 Antenna Width

Width of antenna also plays an effective role in deciding the antenna band width. A decrease in the width of antenna will results in providing a wider bandwidth. According to [4, 12] antenna width should be greater than half of the average value of maximum and minimum operating frequency.

$W > \frac{\lambda min + \lambda max}{4} = \frac{50+150.}{4} = 50mm$ *; So W is taken 80 mm.*

Hence from above statement it can be concluded that a longer length and a small width antenna dimension will result in improving the beamwidth of the antenna.

4.7.4 Mouth opening

It is the outermost part of antenna from which the em wave leaves the antenna structure. There is a bound on the value of opening width [12].i.e. Mouth opening should have a value in between $W_{min} = \frac{\lambda g}{f.\varepsilon}$ and $W_{max} = \frac{\lambda g}{2}$.

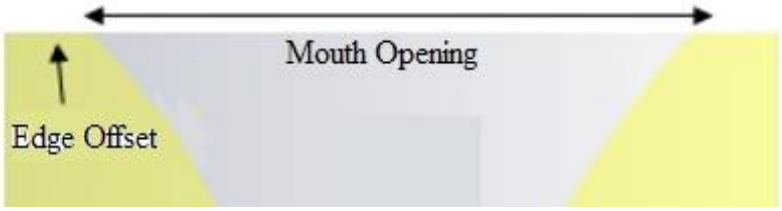

Fig.4.4 Vivaldi antenna's mouth opening.

Where, c = speed of light; *f* min = frequency minimum (2GHz); ε = dielectric constant (2.33). $W_{max} = 49mm$; $W_{min} = 39mm$. Hence an optimum width value is taken i.e. 40 mm.

4.7.5 Edge offset

It is the extra conducting area at the end of the exponential slot. This area offers the freedom to change the return loss and the radiation pattern [12].

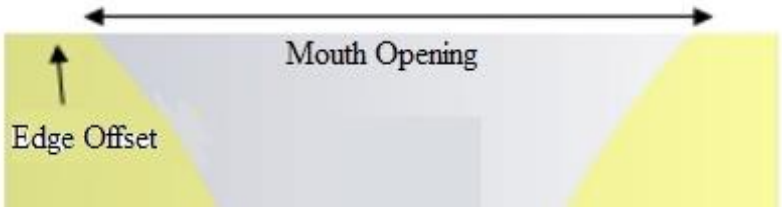

Fig.4.5 The edge offset.

Edge offset can be optimized either by changing the width while keeping the mouth opening constant or by varying the mouth opening while keeping the width constant.

4.7.6 Cavity Diameter

The purpose of circular slot is already explained above. Here cavity diameter is taken as 24 mm.

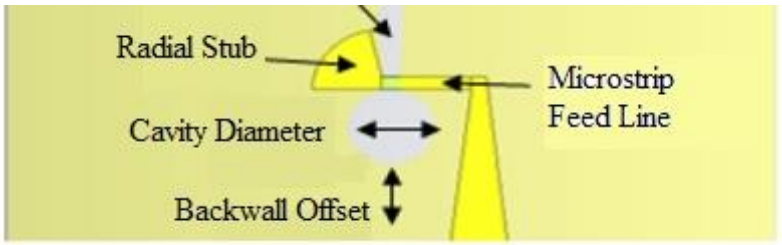

Fig.4.6 The cavity diameter and backwall offset**.**

4.7.7 Exponential Slot

Exponential Slot design is based on two parameters i.e. the exponential length and exponential rate. The exponential slot curve is guided by the following equation:

$$Y = c_1 e^{Rx} + c_2. \tag{4.2}$$

Where $c_1 = \frac{y_2 - y_1}{e^{Rx_2} - e^{Rx_1}}$, and $c_2 = \frac{e^{Rx_2} y_1 - e^{Rx_1} y_2}{e^{Rx_2} - e^{Rx_1}}$ (4.3)

Where R is the exponential rate and x_1, x_2, y_1 and y_2 indicates starting and ending points of the slotline.

4.7.8 Backwall Offset

It is the extended area behind the circular slot of antenna as shown inn figure. This extended area prevents the sudden flow of electrical current which results in offering the freedom to tune the bandwidth of antenna. Here 2.5mm is taken as backwall offset value.

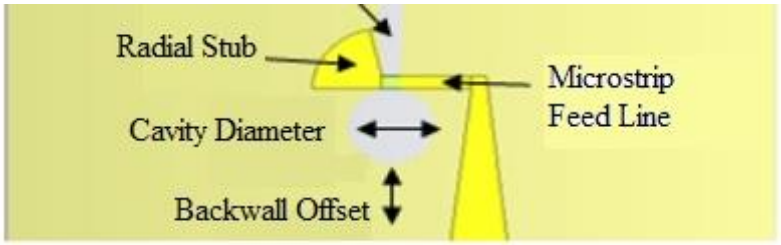

Fig.4.7 The backwall offset.

The above stated numerical results of the Vivaldi antenna dimension will guarantee an excellent performance in terms of gain, directivity and beamwidth.

4.8 Impedance Calculation for Vivaldi Antenna:

In Vivaldi antenna the excitation to rectangular slot is given through a microstrip feed line. A microstrip-slot transition is shown in Fig.4.8 [3]. The slotline and microstrip feed line are etched on different sides of the substrate. Their geometry makes a right angle. Both the microstrip and slotline extends a quarter of wavelength which can be clearly seen in Fig.4.8.

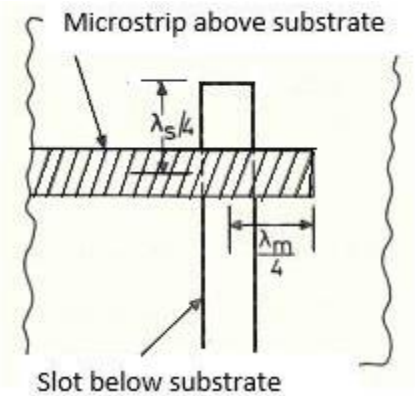

Fig.4.8. Schematic of Microstrip to slotline transition.

An equivalent circuit of the above stated transition is shown in Fig.4.9. X_{OS} represents the inductance of the slotline whereas C_{oc} is the capacitance of an open microstrip. Z_{OS}

and Z_{OM} are slotline and microstrip impedances respectively. θ_S and θ_m represent the electrical lengths of the extended portions of the slotline and the microstrip respectively.

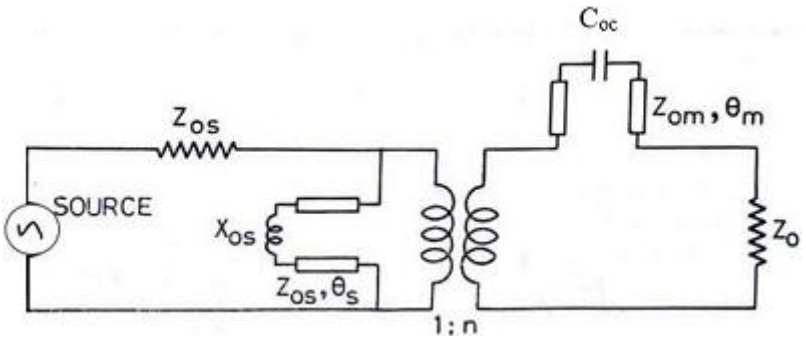

Fig.4.9. Shows equivalent circuit diagram for microstip to slotline transition.

Depending on the dimensions of the transmission line the characteristic impedance Z_0 can be calculated.

For $W/h \leq 1$, $$Z_0 = \frac{60}{\sqrt{\varepsilon_e}} ln\left(\frac{8h}{W} + \frac{W}{4h}\right). \quad (4.4)$$

For $W/h \geq 1$, $$Z_0 = \frac{120\pi}{\sqrt{\varepsilon_e}\left[\frac{W}{h}+1.393+0.667\, ln\left(\frac{W}{h}+1.444\right)\right]}. \quad (4.5)$$

$$\Gamma = \frac{R_S - Z_{OM}}{R_S + Z_{OM}}.$$ Where Γ is reflection coefficient

4.8.1 Equivalent Reflection coefficient for Tapered Slot

Schematic of one side of tapered assembly [1] is shown in Fig.4.10(a), where Z_a is antenna load impedance, Z_0 is characteristic impedance of uniform slotted waveguide, l is total length of exponential profile, β is the propagation constant of the slot line and Γ represents the equivalent reflection coefficient of load impedance at distance l.

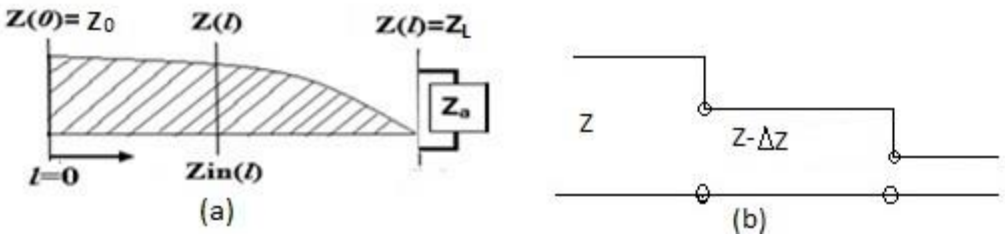

Fig.4.10. (a) Block diagram depicts the impedance variation for Exponential slot w.r.t. length.

(b) Diagram depicts the tapered line composed of decremented sections.

The equivalent of continuously tapered line, as shown in Fig.4.10. (b), is made up of a number of decremented sections of length ΔZ, and then the decremented reflection coefficient from the step z is given by

$$\Delta\Gamma = \frac{(Z-\Delta Z)-z}{(Z-\Delta Z)+z} \cong \frac{\Delta Z}{2Z}, \tag{4.6}$$

Substituting $\Delta Z \rightarrow 0$ for small element the above equation can be written as,

$$d\Gamma = \frac{dZ}{2Z} = \frac{1}{2}\frac{d(lnZ/Z_0)}{dZ}, \tag{4.7}$$

Since,
$$\frac{d\left(lnf(z)\right)}{dZ} = \frac{1}{f}\frac{df(z)}{dz}, \tag{4.8}$$

Using the theory of small reflections, the total reflection coefficient at z=*l* can be calculated by integrating the partial reflections coefficient along with their appropriate phase shifts given by,

$$\Gamma(\theta) = \frac{1}{2}\int_{Z=0}^{L} e^{-2j\beta z}\frac{d}{dZ} ln\left(\frac{Z}{Z_0}\right) dz. \tag{4.9}$$

Impedance of the exponentially tapered section is expressed as,

$$Z(z) = Z_0 e^{az}, \qquad for\ 0 < Z < L \tag{4.10}$$

Value of constant *a* can be determined by applying the boundary condition at $l = 0$, $Z(0) = Z_0$; and L=*l*, $Z(L) = Z_L = Z_0 e^{aL}$, as shown in Fig.4.10. (a)

$$a = \frac{1}{L} ln\left(\frac{Z_L}{Z_0}\right), \tag{4.11}$$

By putting the value of Z/Z_0, the reflection coefficient is written as,

$$\Gamma = \frac{1}{2}\int_{Z=0}^{L} e^{-2j\beta z}\frac{d}{dZ} ln(e^{az}) dz, \tag{4.12}$$

This gives,
$$\Gamma = \frac{lnZ_L/Z_0}{2} e^{-j\beta L}\frac{\sin\beta L}{\beta L}. \tag{4.13}$$

Hence equation (4.13) shows a relation between the reflection coefficients, Γ at any arbitrary location *l* on tapered profile. On the basis of this relation, length and exponent of the slot profile can be calculated for the defined values of Γ and $Z_L = 50\Omega$.

Chapter 5

Parametric Study and Designing of Vivaldi Antenna on Comsol

5.1 Parametric Study on designing parameters

A parametric study is done before designing Vivaldi antenna. The effect of variation of radiation parameter is studied for circular slot as well as exponential slot whereas keeping all other parameters constant. The parametric study enables to decide an exact value for the circular cavity's diameter and exponential slot's length and exponent constant by comparing the S_{11} parameter and polar plot of radiation pattern.

5.1.1 Parametric study for the Diameter of the Circular Slotline Cavity

The circular cavity offers to tune the impedance of the Vivaldi antenna [12]. The parametric variation of the circular slotline cavity is studied with the other parameters fixed.

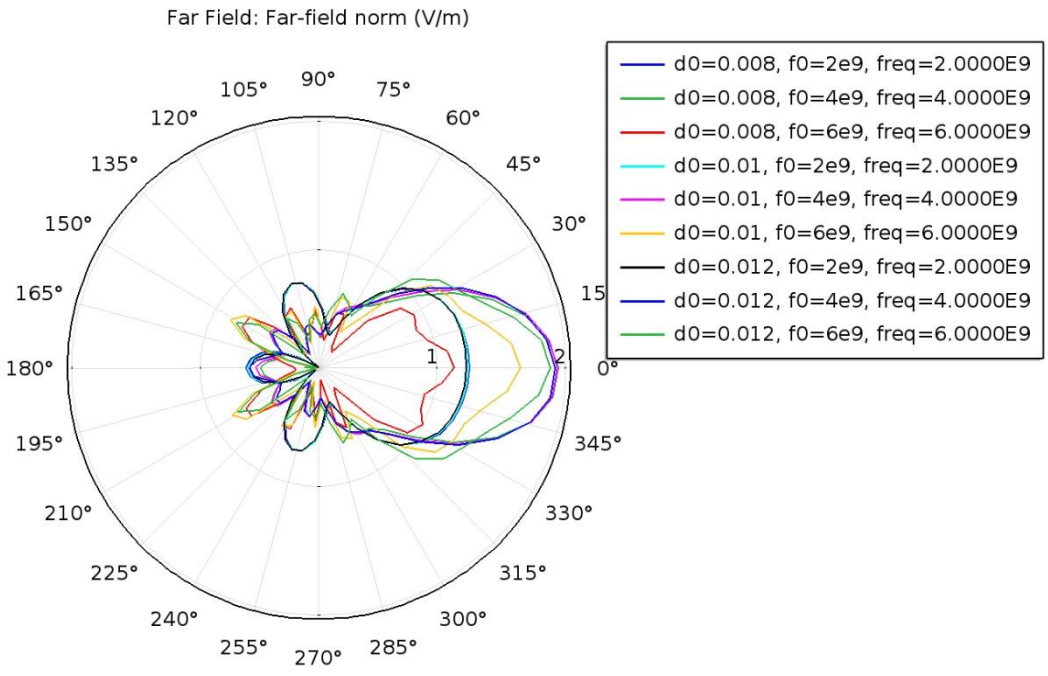

Fig.5.1 Polar plot response for varying cavity diameter against frequency.

The radius of the slotline is varied from 8mm to 12 mm and the results are shown in Fig.5.1. From the simulated results it is verified that the antenna shows high

directionality and effective impedance matching at a radius of 12mm corresponding to a frequency of 6GHz. At this frequency beam width as well as S_{11} is seen to be minimum as shown in Fig.5.1 and Fig.5.2 respectively.

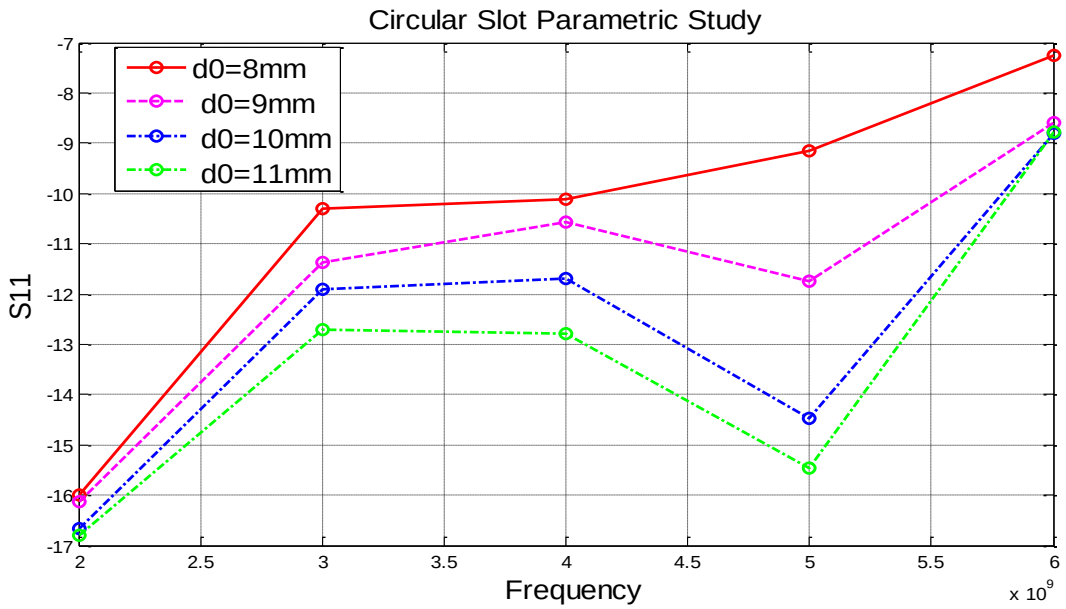

Fig.5.2 S_{11} response for varying cavity diameter against frequency.

The antenna is simulated at different radius of circular slot. From the exact behavior of beamwidth pattern and S_{11} response, one can easily interpret that there is an inverse relationship between the circular cavity diameter and S_{11} value. Increase in diameter of slot results in lower S_{11} value. It is also seen that minimum beamwidth is obtained at 12mm cavity radius.

5.1.2 Parametric study for the exponent of exponential slot

The opening rate of the tapered slotline is found to affect mainly affect the mid-band performance of the TSA. In this section, the exponential rate 0.044*x, where 'x, is varied from 0.25 to 1. Exponential slot is guided by the equation. y= $\pm c_1 e^{Rx} + c_2$; where c_1 and c_2 are calculated by using the end points in above equation.

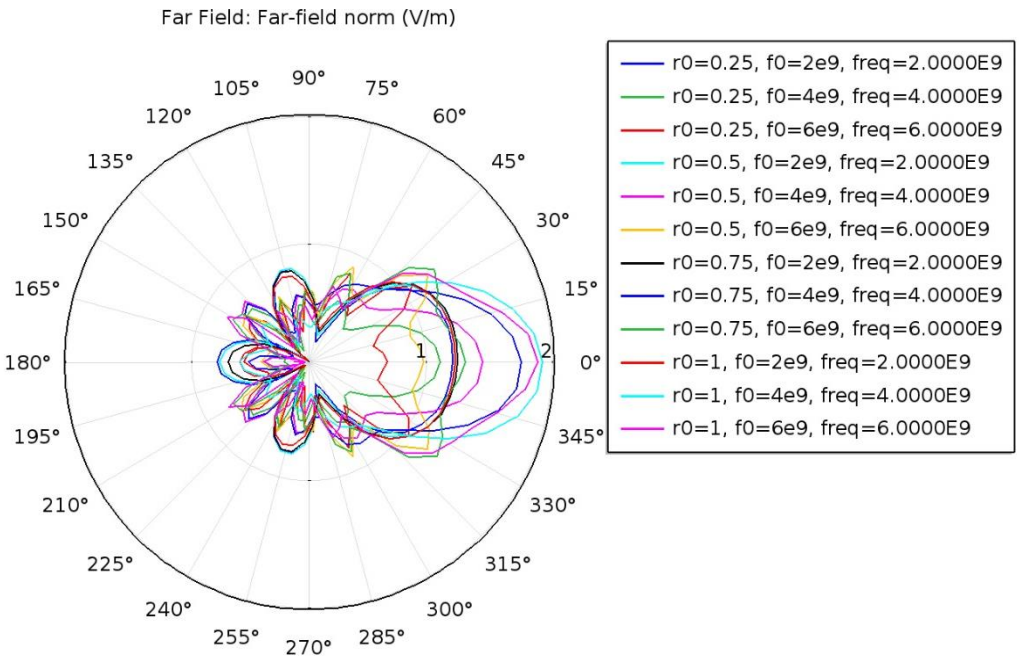

Fig.5.3 Polar plot response for varying exponent constant against frequency.

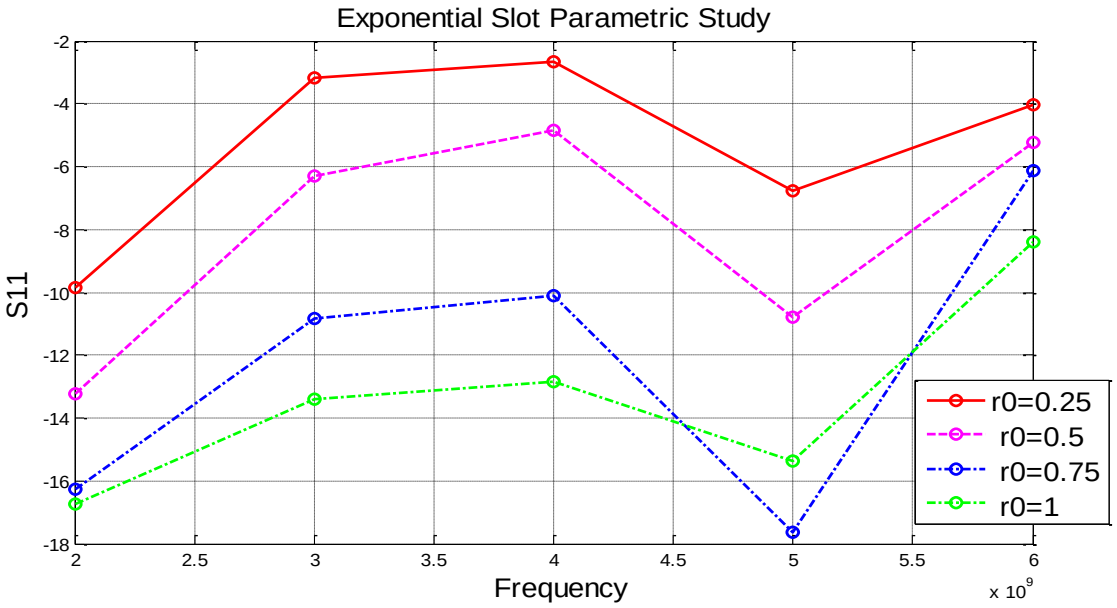

Fig.5.4 S_{11} response for varying exponent constant against frequency.

From the above Fig.5.3 and Fig.5.4, it is observed that for a frequency of 6GHz at an exponent value of 0.044, the radiation pattern is more directional and minimum return loss of 18dB is obtained. It can be concluded that as the rate of exponential slot increases, there is a wide increase in the beam width of antenna. As the wave guides along the curves of the exponential slot, it can be concluded that beamwidth is dependent on the rate of exponential slot.

5.2 Design Specifications

The dimensions are evaluated and optimized using COMSOL Multiphysics software and Fig.5.5 shows the comprehensive prototype of Vivaldi antenna. The dimensions of antenna slot profile is given on PCB base. A sector-shaped terminated area on microstrip feeding line is used to excite the circular slot of antenna as shown in Fig.5.5 (a). Signal couples with the circular resonant slot via capacitive coupling from the back side of PCB plane to the front side and reaches to the aperture end through a symmetrical exponential slot followed by a rectangular slot line as shown in Fig.5.5 (b).

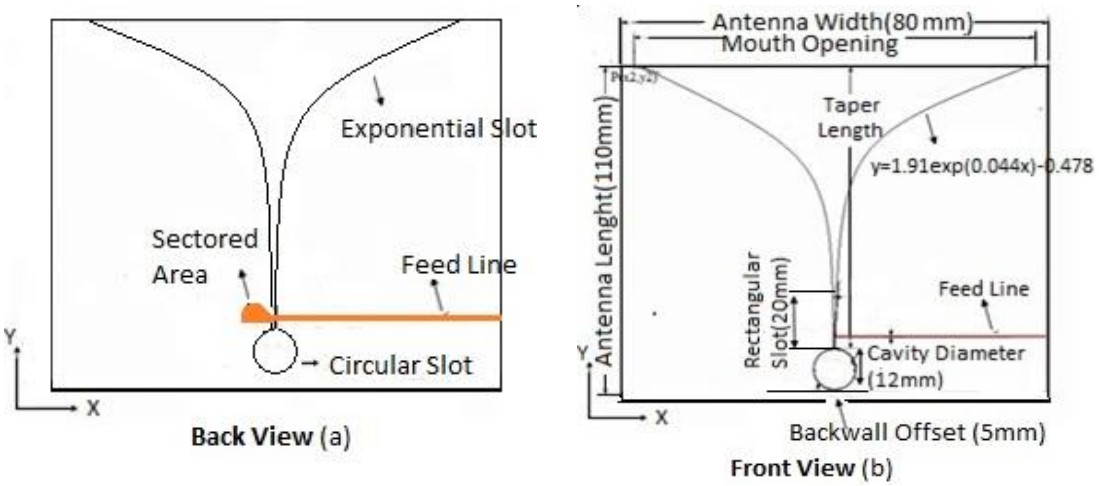

Fig.5.5. (a) Back View of Vivaldi Antenna showing feedline and different types of slots.

(b) Drawing shows parametric values taken while designing Vivaldi Antenna.

5.3 Simulation

The entire model is designed and simulated on COMSOL Multiphysics software. In this the Vivaldi Model is enclosed by a perfectly matched layer (PML). The PML layer fulfills the work of an anechoic chamber. This chamber results in absorption of all the radiated energy beyond its boundary. Hence this chamber helps in evaluating the far field gain, directivity and other performance parameters of antenna. In Fig.5.6 the shaded area in blue represents the PML layer surrounding the antenna at a far field distance. From the legend color coding it can be evaluated that all the radiated wave is being absorbed at its boundary.

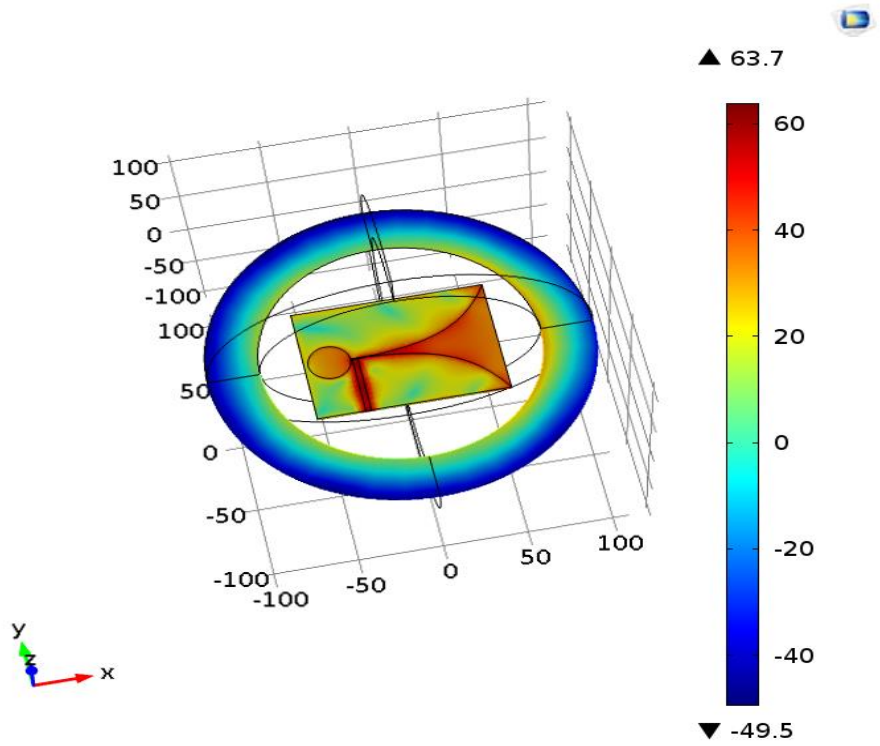

Fig.5.6 Shows em wave traveling from microstrip to exponential slotline.

In this model a Vivaldi Antenna is designed on a thin dielectric substrate. The curves of the exponential slot are patterned with a PEC layer.

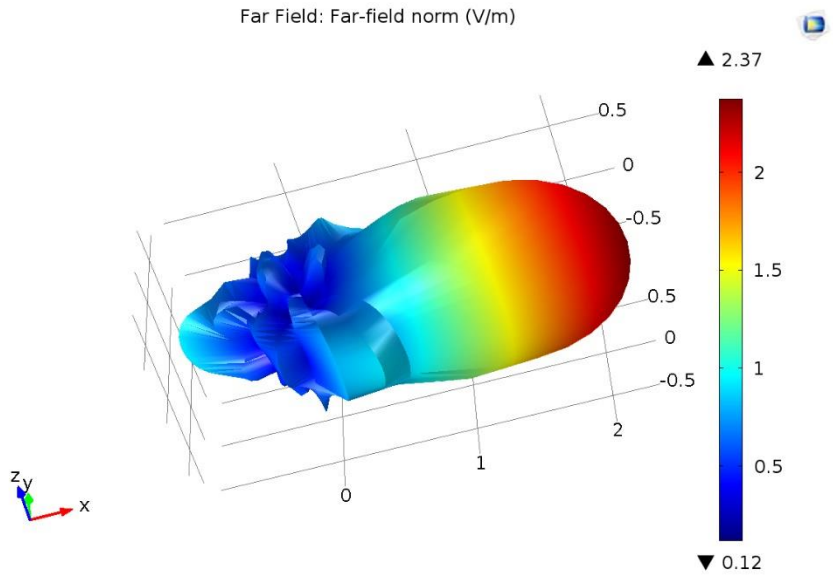

Fig.5.7 A 3-D view of the Far-filed radiation pattern of Vivaldi antenna.

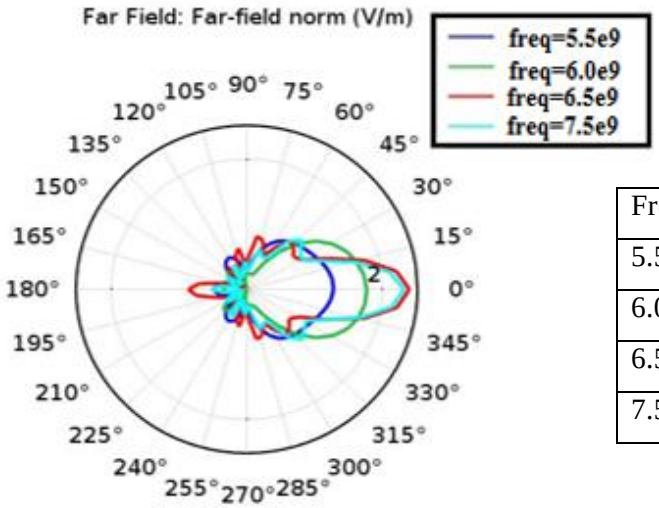

Frequency	Directivity
5.5 GHz	1.9322
6.0 GHz	2.7883
6.5 GHz	3.7504
7.5GHz	3.7884

Fig.5.8 Show a 2-D polar plot of radiation pattern of Vivaldi antenna.

The above polar pot in Fig.5.8 shows the major lobe radiation pattern. The plot gives the information about the directivity variation with respect to frequency variation. It can be analyzed that as the frequency increase the major lobe is getting more directive in nature.

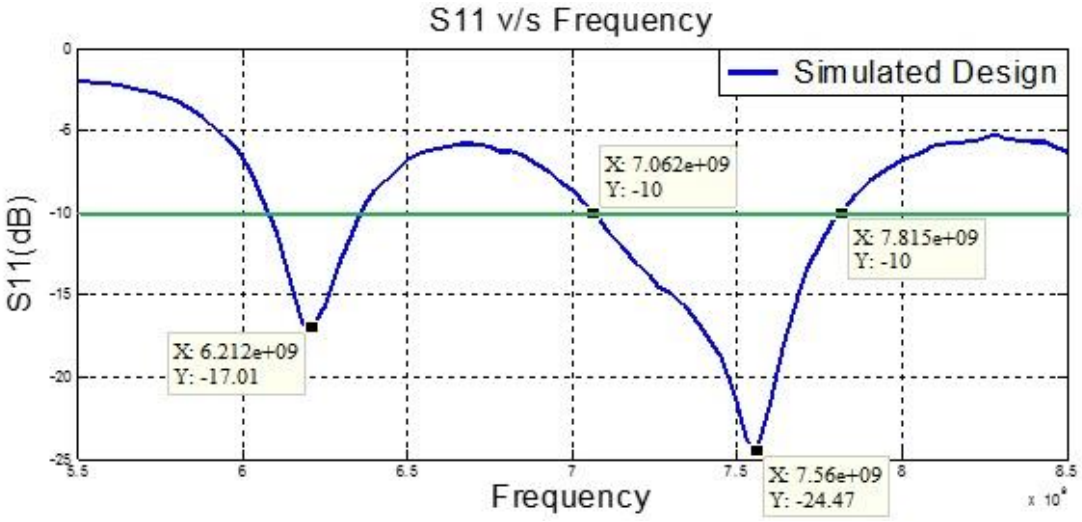

Fig.5.9 Plot representing S11 of Vivaldi Antenna Design simulated on COMSOL.

Simulation result are plotted in terms of radiated electric field, polar plot and S_{11} in Fig.5.7, Fig.5.8 and Fig.5.9 respectively which are explained as; the far field plot represent a directive end-fire radiation pattern of the Vivaldi antenna toward the wide end of its tapered slot. The operating frequency of Vivaldi antenna is 7.5GHz and it is providing 15dB bandwidth in frequency range of (5.5-8.5) GHz.

Chapter 6

Fabrication of Vivaldi Antenna on PCB

6.1 Vivaldi Design Implemented on PCB FR4 substrate

The above simulated model is fabricated on a PCB alumina substarte with dielectric constant of 4.33 and substrate thickness of 1.5mm. PCB substarte is coated with a very thin layer of alumina (1.5microns approx.) which has been itched as per dimension of the simulated prototype. Fig.6.1 shows the front and back view of fabricated vivaldi antenna. The front view describes the main design of antenna PCB whereas backview of PCB, shows the feed line. A sector shaped area is fabricated at end of the fed line in order to provide the capacitive coupling soo that the em wave can couple from the back to front of PCB substrate.

Fig.6.1. The diagram shows the front and
back view of Vivaldi antenna fabricated on PCB.

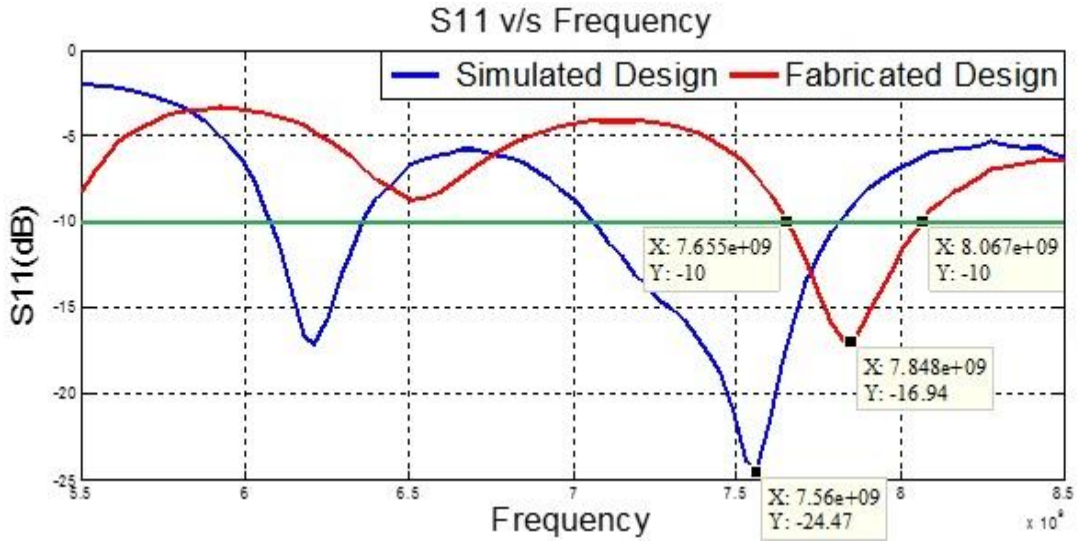

Fig.6.2. S11 Comparisoin plot for the Fabricated design with Simulation Design.

Vector Network Analyser (VNA) is used to test the fabricated design where a comparitive plot of S_{11} between test and simulation result is shown in Fig.6.2. The comparison shows that in prescribed band, the return loss of fabricated antenna is not found in good agreement with the simulation result. This ambiguity has been analysed and found associated to the discontinuity present at feeding lines, fabrication constraint and bent of micro-stripline which introduce the parasitic reactance in antenna design. A theoratical procedure has been developed to compensate and implemented in fabrication in order to improve the performace i.e. explained in next chapter.

Chapter 7

Compensation using reactive patch on feeding line

7.1 Implementation of compensation in fabrication

Further study reveals that the mismatching of antenna is related to the cause of discontinuity at feeding point, fabrication tolerance and associated parasitic capacitance at edges or bent of micro-stripline which introduce the parasitic reactance in antenna design [34, 35]. Thus, the antenna impedance is mismatched from the RF source which should be essentially matched for the better radiation. For this reason test result is found deteriorated from the simulation results. Here, a theoretical procedure has been developed for the compensation of the associated problems. The theory explores that the mismatching of antenna can be compensated by using a reactive patch on feed lines. The patch is small segment of the stripline that introduces reactive equivalence in feed line. The patch introduces an additional impedance that transfers to the antenna impedance. This concept is used to improve the mismatching of antenna. Two different types of patch are studied i.e. inductive and capacitive patch in this section. Both the patches are compared with the uncompensated technique and a generalized theory is given that can be used in fabrication of antenna to get desired results without changing the original design.

7.2 Equivalent circuit diagram for the reactive patch

From equation (7.6) it can be observed that introduction of patch in the microstrip line induces a variation in the equivalent inductive and capacitive values [36]. These variations result in changing of the antenna impedance. Hence this concept plays a significant role in matching the impedance of microstrip line with slotline.

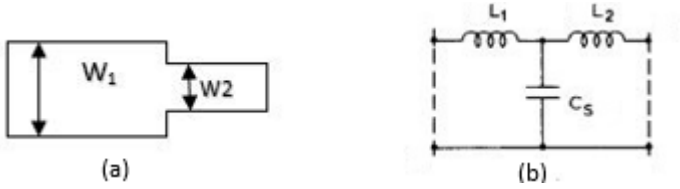

Fig.7.1 (a) Shows the layout of reactive patch in the feed line.
(b) Represents the equivalent circuit diagram of reactive patch.

$$\frac{C_s}{\sqrt{W_1 W_2}}\left(pF/_m\right) = (10.1\log\varepsilon_r + 2.33)\frac{W_1}{W_2} - 12.6log\epsilon_r - 3.17. \quad (7.1)$$

$$\frac{L}{h}\left(nH/_m\right) = 40.5\left(\frac{W_1}{W_2} - 1.0\right) - 75log\frac{W_1}{W_2} + 0.2\left(\frac{W_1}{W_2} - 1\right)^2. \quad (7.2)$$

Fig.7.1 (a) and Fig.7.1 (b) shows the layout of the design of patch which is to be incorporated in feedline and the equivalent circuit diagram for the same respectively. The equation (7.1) and equation (7.2) shows a relation of effective capacitance and inductance with varying width of the patch. Hence this shows a theoretical model for the effective capacitive and inductive values for the patch compensation in feed line. Two different compensated techniques are applied, briefly explained and studied in the next section i.e. capacitive and inductive patch. Both the patches are compared with each other and the effective compensation technique is taken for the incorporation in fabrication of antenna

7.3 Use of capacitive patch for compensation

First use of capacitive loaded feed line is incorporated in the design to compensate the above stated problems. An equivalent circuit of antenna including source, feed line and patch is shown in Fig.7.2 Here antenna impedance is taken as Z_A which is different from the impedance of feed line Z_0=*50*Ω. Here, Z_C is the transferred impedance of antenna on feed line. A stripline patch of length $l = \lambda/4$ and impedance Z_P is introduced in feed line for compensation of antenna impedance.

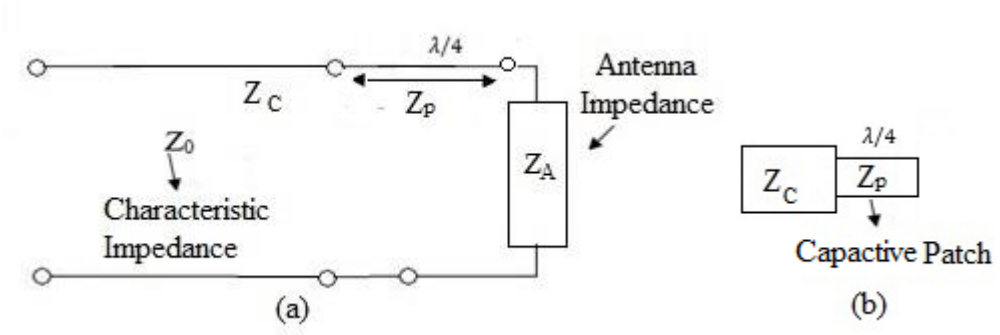

Fig.7.2 Block Diagram depicts the Impedance offered by reactive path of Antenna feedline.

Here impedances Z_p is normalized at characteristic impedance Z_0. For a quarter length of matching section patch, Z_C can be expressed as,

$$Z_C = \sqrt{Z_P}, \tag{7.3}$$

Where,

$$Z_p = {}^{1}/_{wc_{eff}}. \tag{7.4}$$

From equation (7.4), it can be observed that the patch behaves as capacitive and introduces reactance of $\sqrt{Z_P}$, that is added to the antenna impedance and can be changed by changing any one of parameters, Z_p and *l*. Thus, antenna can be matched by compensating the reactive patch.

7.3.1 Implementation of capacitive reactive patch in fabrication

The procedure stated in chapter 7.3 provides a method by which the compensation of antenna can be made without affecting the original design of antenna. This theory has been applied for the compensation of associated problem in design of Vivaldi antenna and incorporated in fabrication. The photograph of compensated antenna is shown in Fig.7.3, where a small patch is fabricated on feedline.

Fig.7.3 Capacitive compensated Vivaldi antenna design.

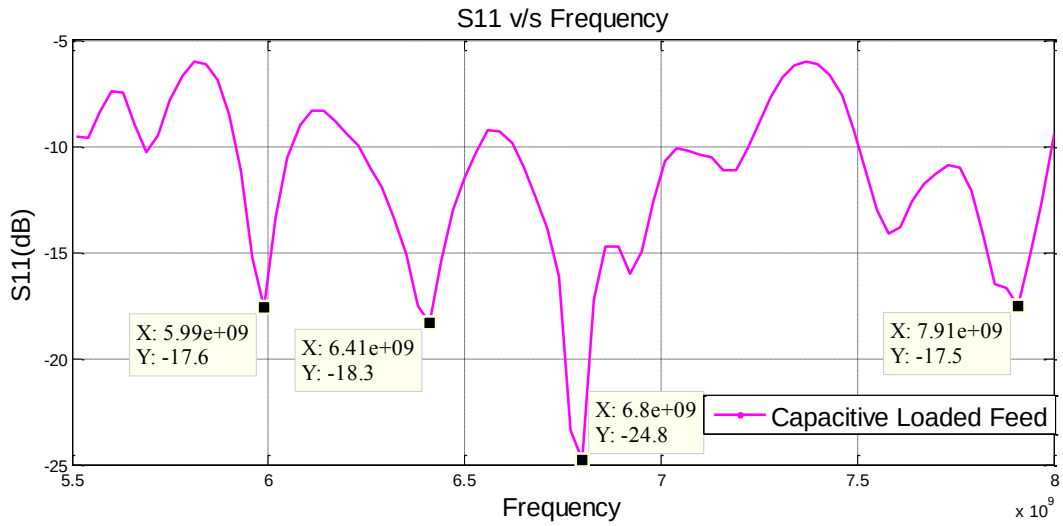

Fig.7.4 S_{11} plot for capacitive loaded feed line.

The S_{11} plot in Fig.7.4 shows that the antenna is showing a return loss of 24.8dB at a frequency of 6.8 GHz. Here, the introduction of capacitive load in feedline provides nearly 15dB bandwidth.

7.4 Use of inductive patch for compensation

An equivalent circuit of antenna including source, feed line and patch is shown in Fig.7.5. Here antenna impedance is taken as Z_A which is different from the impedance of feed line Z_0=50Ω. Here, Z_B and Z_C are transferred impedance of antenna at point *B* and *C* on feed line respectively. A stripline patch of length $l = \lambda/12$ and impedance Z_P is introduced in feed line for compensation of antenna impedance where impedance ,$Z_P$is taken as $\gg Z_B$.

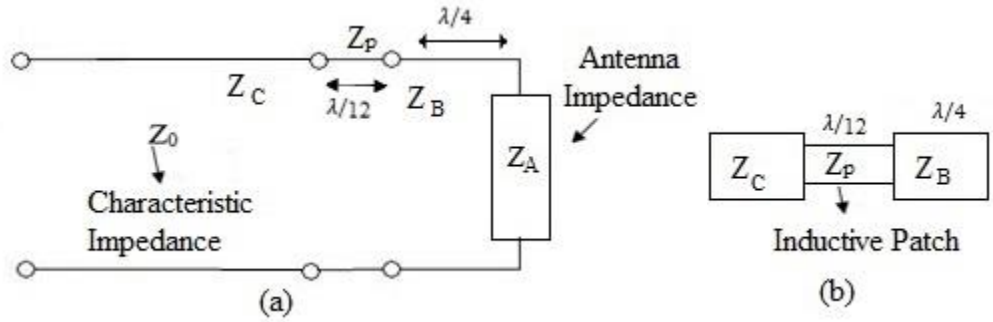

Fig.7.5 Block Diagram depicts the Impedance offered by reactive path of Antenna feedline.

From Fig.7.5 (a) Z_B and Z_C can be expressed as,

$$Z_B = \sqrt{Z_A}, \tag{7.5}$$

$$Z_C = Z_p \left(\frac{Z_B + jZ_p \tan(\beta l)}{Z_p + jZ_B \tan(\beta l)} \right), \tag{7.6}$$

Here impedances Z_A and Z_B are normalized at characteristic impedance Z_0.

For $l < \lambda/10$, and $Z_B \ll Z_p$, term $tan\beta l \approx \beta l$, is incorporated in equation (7.6),

$$Z_C = Z_p \left(\frac{Z_B + jZ_p(\beta l)}{Z_p + jZ_B(\beta l)} \right). \tag{7.7}$$

The above can be approximated for $Z_p \gg Z_B \tan(\beta l)$, now

$$Z_C = Z_p \left(\frac{Z_B + jZ_p(\beta l)}{Z_p} \right), \tag{7.8}$$

$$Z_C = Z_B + jZ_p(\beta l). \tag{7.9}$$

From equation (7.5) and (7.9)

$$Z_C = \sqrt{Z_A} + jZ_p(\beta l). \tag{7.10}$$

From equation (7.10), it can be observed that the patch behaves as inductive and introduces reactance of $Z_p(\beta l)$ that is added to the antenna impedance and can be changed by changing any one of parameters, Z_p and l. Thus, antenna can be matched by compensating the reactive patch.

7.4.1 Implementation of inductive patch in fabrication

The procedure stated in chapter 7.4 provides a method by which the compensation of antenna can be made without affecting the original design of antenna. This theory has been applied for the compensation of associated problem in design of Vivaldi antenna and incorporated in fabrication. The photograph of compensated antenna is shown in Fig.7.6, where a small patch is fabricated on feedline.

Fig.7.6 Fabricated design of Vivaldi Antenna (a) front view.
(b) Back view showing feeder with Compensation (Inductive Patch on feedline).

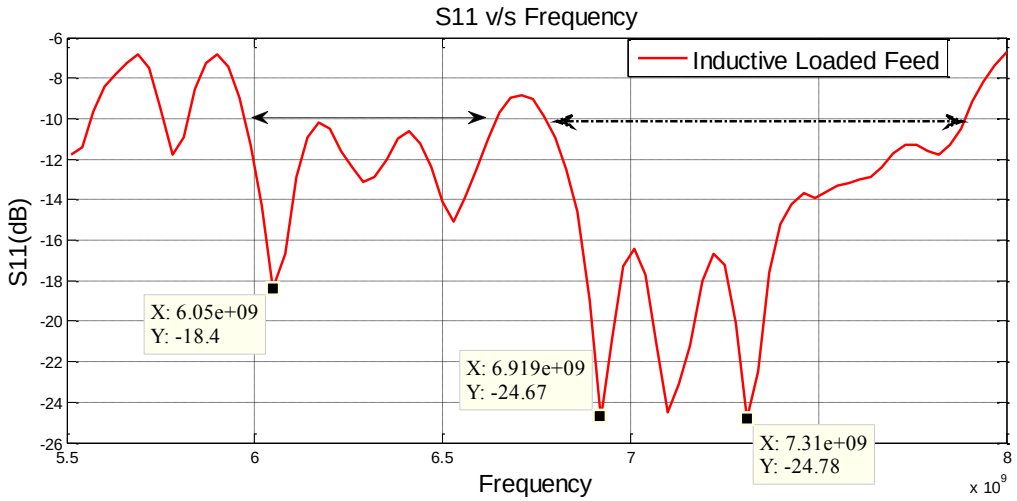

Fig.7.7 S_{11} plot for the inductive loaded feed line.

From Fig. 7.7 it can be observed that the antenna is resonating at two frequencies i.e. 6.05GHz and 7.31GHz and also showing a wideband behavior. The respective return loss are also nearly greater than or equal to 24.78dB. On comparison of both the S_{11} plot of capacitive and inductive loaded antenna Fig.7.4 and Fig.7.7, it can be concluded that inductive loaded antenna's performance is much better than the capacitive loaded antenna. Hence inductive loaded feedline is used as a compensation technique and incorporated in antenna design for fabrication.

7.5 Results and Discussion

The proposed compensation has been incorporated in fabrication of antenna and is tested with Vector Network Analyser (VNA). Test and simulation results are shown in Fig.7.8 in comparative manner. As it is observed in section 6.1 that in the given frequency band, the center frequency of uncompensated antenna is shifted right side and overall return loss parameter, S_{11} is found inferior in comparison with simulation result. The bandwidth of uncompensated antenna, B_2 i.e. 7.65-8.06GHz also found narrow as compared to the simulation result B_1 i.e. 7.06-7.81GHz.

As the compensation in feed line is incorporated, the test result is found providing better return loss parameter in entire frequency band as compared to the simulation and test result of uncompensated antenna as well. Here center frequency is also found shifted toward left side and provide wider bandwidth B_3, i.e. 6.77-7.89 GHz as compared to B_1 and B_2. This also covers the desired operating band B_1 along with center frequency i.e. 7.5 GHz as we get in simulation result. As we observe that applied compensation not only provide better return loss but also shift the frequency band in desired range. The parameters that are achieved in compensated antenna are compared with simulation result and test result of uncompensated antenna and shown in Table1 in perspective manner.

Table1. Comparative observation deduced on the basis of S_{11} Plot.

Antenna	Frequency Range (GHz)	Center Frequency (GHz)	S_{11} (dB)	Fractional Band-width	%age Band-width
Simulated Design	B_1 (7.06-7.81)	7.56	-24.5	0.0992	9.92%
Fabricated Design without Compensation	B_2 (7.65-8.06)	7.86	-16.94	0.0521	5.21%
Fabricated Design with Compensation	B_3 (6.77-7.89)	7.31	-24.8	0.1532	15.32%

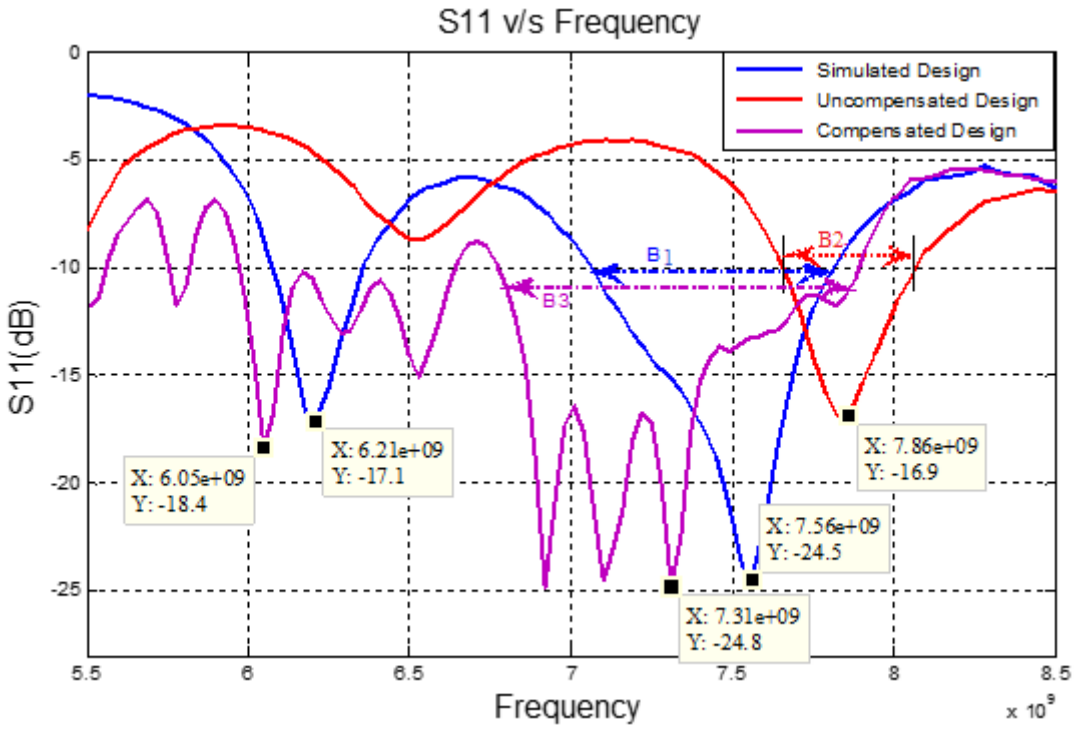

Fig.7.8 S_{11} plot for the Compensated Designs plotted against Conventional Design.

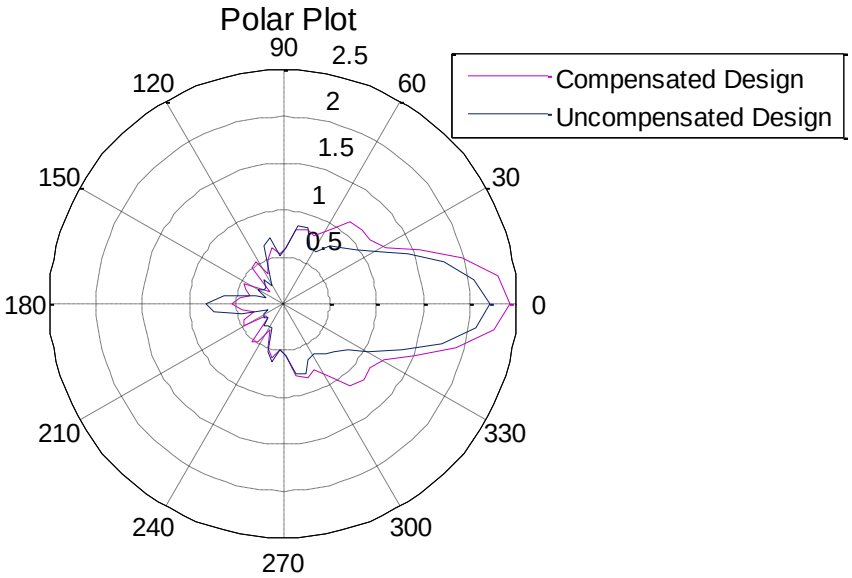

Fig.7.9 Radiation pattern plot for Compensated design plotted against uncompensated design.

Here Fig.7.9 shows the comparison of simulation results of compensated and uncompensated antenna in terms of polar plot. It can be obesrved that inclusion of patch in antenna improves the performance of the antenna in terms of gain and beamwidth which become more wider.

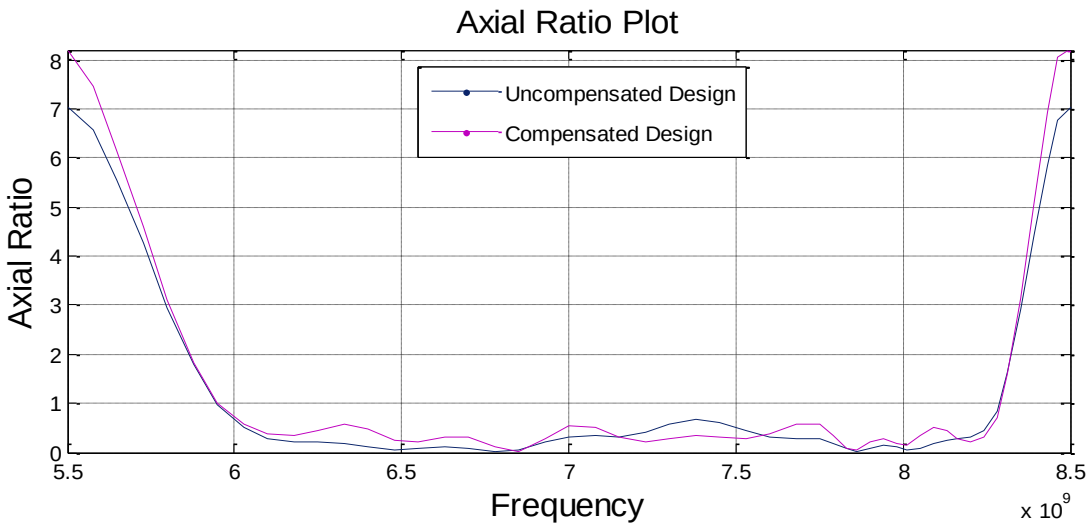

Fig.7.10. Axial Ratio plot for Compensated design plotted against uncompensated design.

Fig.7.10 repersents the axial ratio plot for the uncompensated and compensated antenna design. Here one can observe that the axial ratio for both are found similar in the band. This means, patch compensation does not affect polarisation.

Chapter 8

Vivaldi Antenna enclosure in Radome Chamber

8.1 Brief overview of Radome

A radome acts as an enclosure around antenna, thereby protecting it from the environment. Moreover, the radiation characteristics such as antenna directivity can also be improved with it. From the results it can be easily observed that the radome results in overall improving the gain as well as radiation parameters of a Vivaldi antenna [37]. A radome is a portmanteau of radar and dome. Material used for construction of radome minimizes the attenuation of the em signal during transmission. In nutshell, the radome boundary behaves like a transparent layer for the radar as well as radio waves. Further it also protects the antenna structure from environmental hazards like weather along with it also hides the electronic and sensitive components from the site of public.

Radomes can be made in various shapes (spherical or cylindrical or planar) depending on the specific application by using different materials like fiberglass or PTFE-coated fabric. Keeping in mind the properties of Radome Chamber, the concept is used to increase the performance of Vivaldi antenna by enclosing it into the Radome Boundary.

8.2 Model Definition

The model shown in Fig.8.1 represents the radome enclosing a Vivaldi antenna. A double layered dielectric lens is placed which confines the fields to increase the antenna gain. In this Vivaldi antenna model, the tapered slot profile is designed above the dielectric substrate with a PEC plane which is grounded. A simple exponential function, $e^{0.044x}$ is used to create the tapered slot curves. One end of the slot is open to air and the other end is finished with a circular slot. The feeder having the property of PEC surfaces is designed on the bottom of the substrate. The entire structure is enclosed in a cylindrical PTFE housing, capped by a half-spherical shell. Within this, a half-sphere of a quartz glass dielectric is used to increase the antenna gain. The PTFE housing is backed by a metal housing, also modeled as PEC surfaces. The entire antenna structure is modeled within a sphere with the properties of vacuum and operated at a frequency of 5GHz.

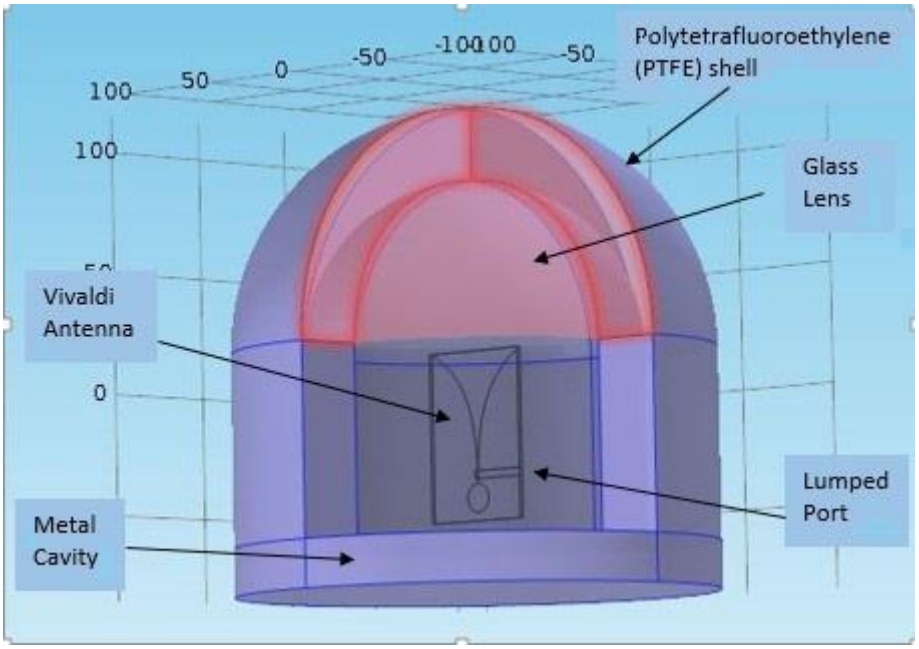

Fig.8.1 A Vivaldi Antenna enclosed by a Radome boundary.

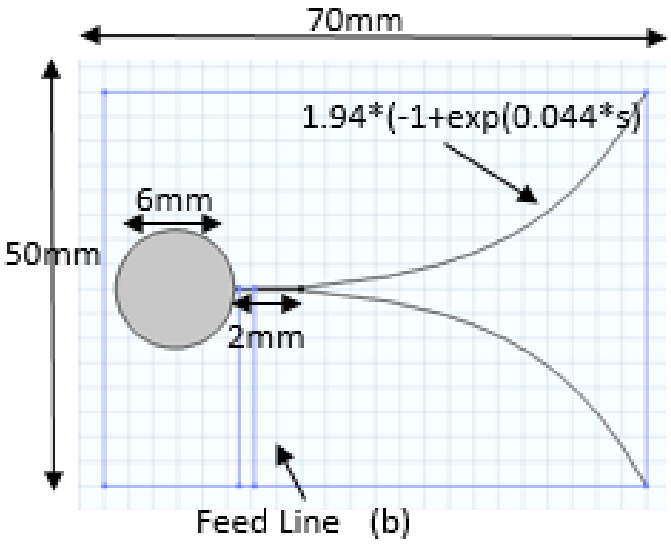

Fig.8.2. Prototype of Vivaldi Antenna Design.

This sphere is truncated by a perfectly matched layer (PML) domain that acts as a boundary to free space. The distance from the antenna to the PML is a variable that is governed by the Far field equation. The thickness of the PML itself is not critical, and can be made approximately one tenth of the air sphere diameter. The meshing of radiating structures requires some care. As a rule of thumb, use it at least five elements per wavelength in each material, although if absolutely necessary, as few as three elements [38]. Furthermore, curved edges and surfaces are meshed with at least two

elements per 90° chord, and the stricter of the two criteria are used. Additionally, tetrahedral elements of approximately unit aspect ratio is used, with the exception of the PML domains. Because the PML domain preferentially absorbs radiated energy in one direction. Hence a swept mesh is thus used in PML region.

8.3 Design Parameters

Following are the parameters that are taken into consideration while designing the Vivaldi Antenna inside a radome.

Table 2. Listing all the parameters in the modeled design.

Name	Expression	Description
Thickness	60[mil]	Substrate thickness
w_slot	0.5[mm]	Slot with
c_slot_radius	5[mm]	Circular Slot Radius
Height	70[mm]	Height of Antenna
Width	50[mm]	Width of Antenna
f0	5[GHz]	frequency in sweep
lda0	c_const/f0	Current wavelength
h_max	0.2*lda0	Max. element size
r_radome	100[mm]	Radome radius
h_radome_wall	80[mm]	Radome wall height
t_radome_bottom	20[mm]	Radome bottom thickness
t_radome_wall	30[mm]	Radome shell thickness

8.4 Results and Discussion

The entire simulation is done on 5GHz of frequency. The radiated power is plotted in its polar coordinates. This variation of power density in terms of its angular coordinates is graphically represented and termed as radiation pattern. The Efar-field radiation pattern is shown in Fig.8.3. It shows that the E-fields that are confined through the radome structure, result in stronger fields at the centre of the top shell. This shows that a radome can work as an antenna enclosure and hence improve the antenna directivity. Fig.8.4 depicts the polar plot of E-fields at far field distance. It reveals that the antenna

enclosed in the Radome boundary results in more directive E-field in comparison to conventional design.

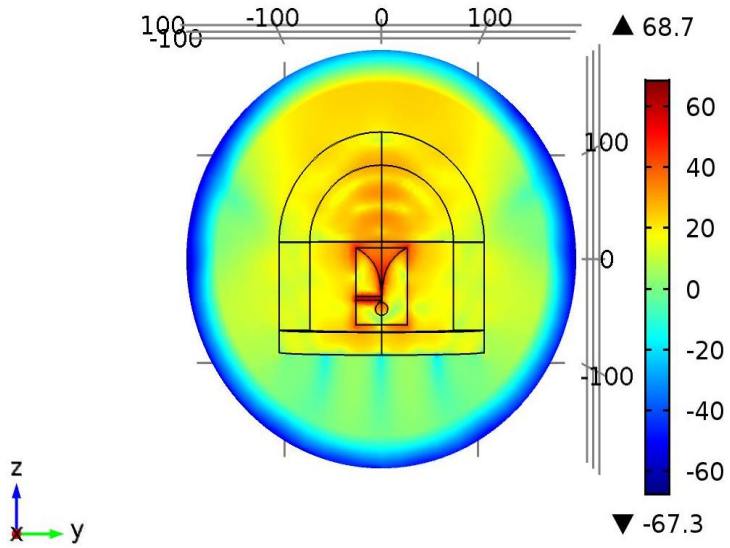

Fig.8.3 Simulated E-field distribution on the radome shell.

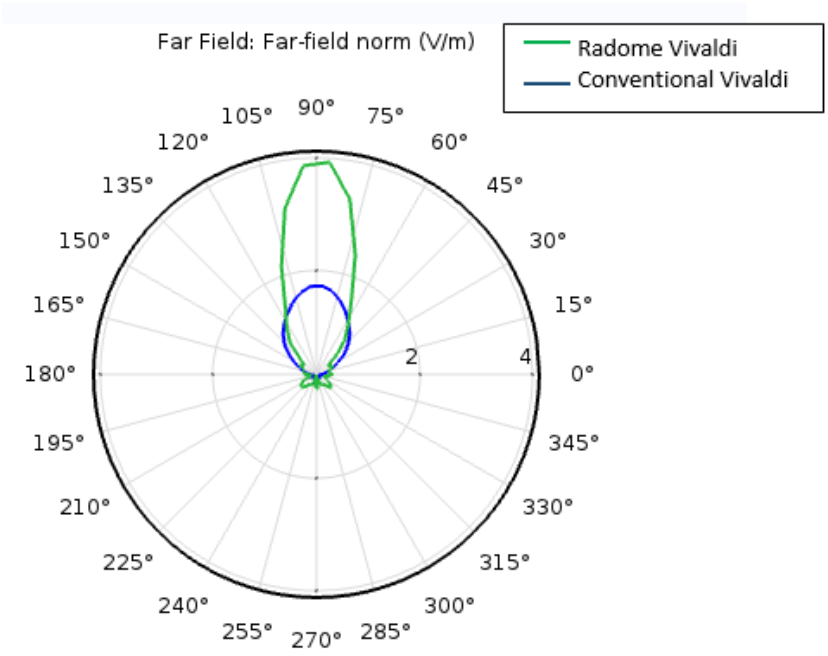

Fig.8.4 Simulated Polar Plot of Vivaldi with and without Radome Boundary.

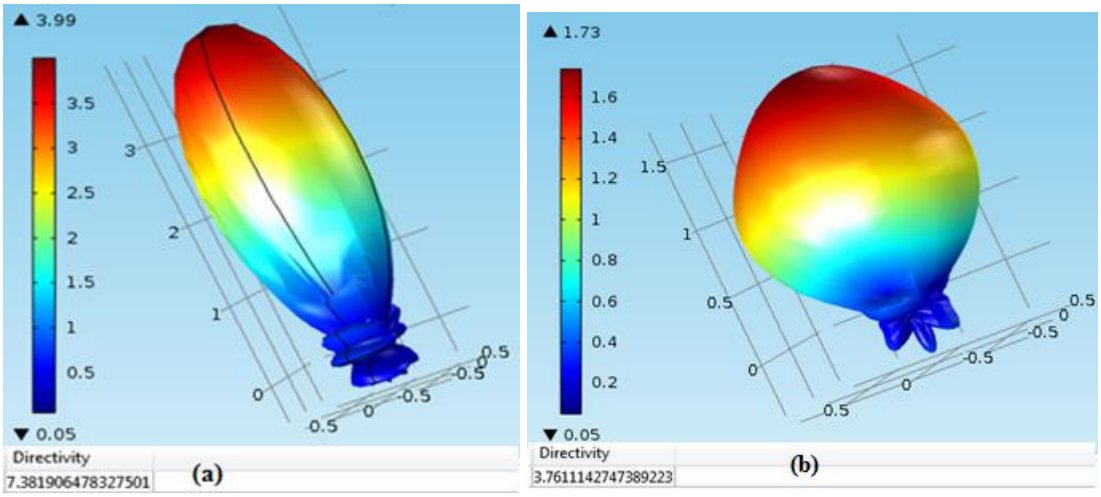

Fig.8.5 The 3D far-field radiation pattern of Vivaldi Antenna
(a) with Radome Boundary (b) without Radome Boundary.

The 3-D Far Field Radiation pattern reveals that the Vivaldi antenna having the Radome boundary is more directive as compared to that of conventional Vivaldi Antenna. The directivity values are 7.38 and 3.76 respectively which are shown in 3D Far field radiation pattern as in Fig.8.5 (a) and (b) respectively.

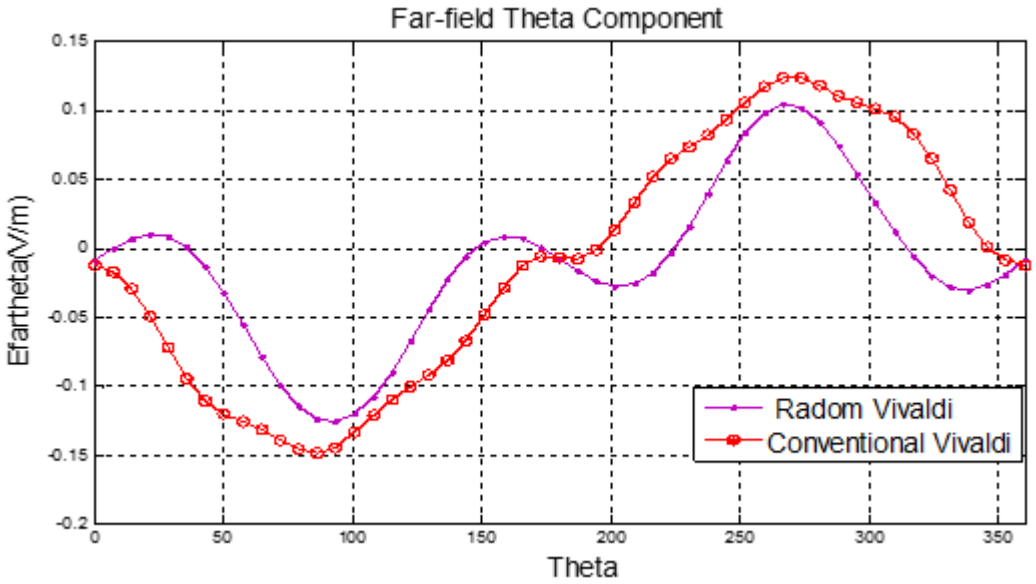

Fig.8.6 Simulated E-Far Field (V/m) against Theta Component
of Vivaldi Antenna with and without Radome Boundary.

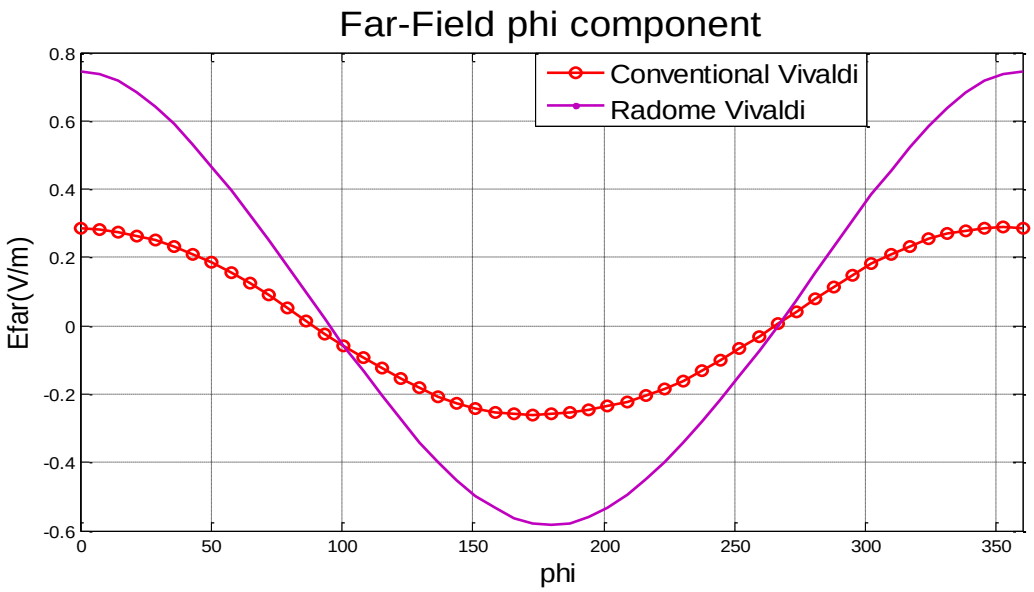

Fig.8.7 Simulated E-Far Field (V/m) against Phi Component of Vivaldi Antenna with and without Radome Boundary.

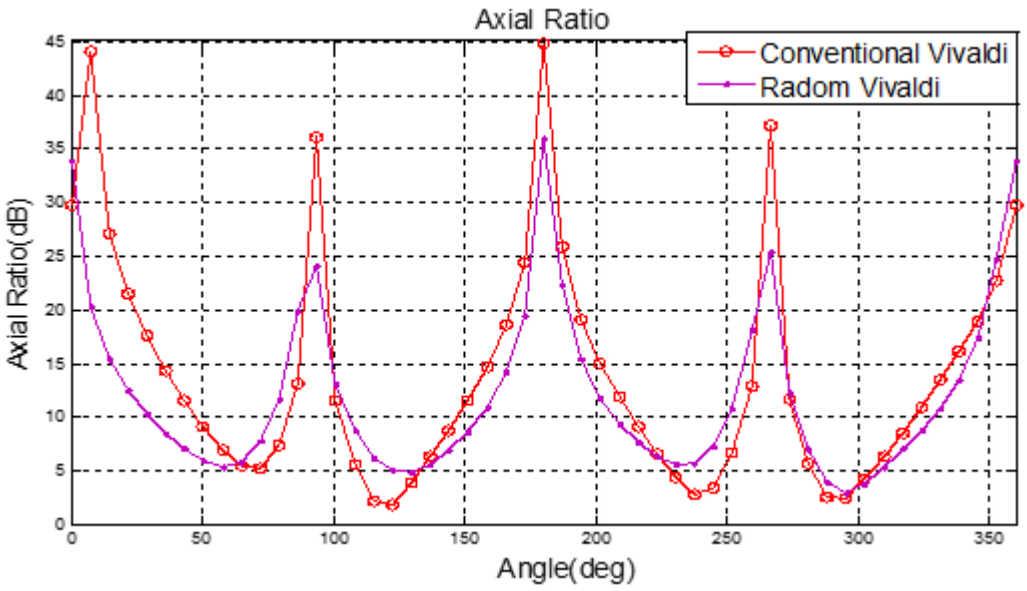

Fig.8.8 Simulated Axial Ratio Plot of Vivaldi Antenna with and without Radome Boundary.

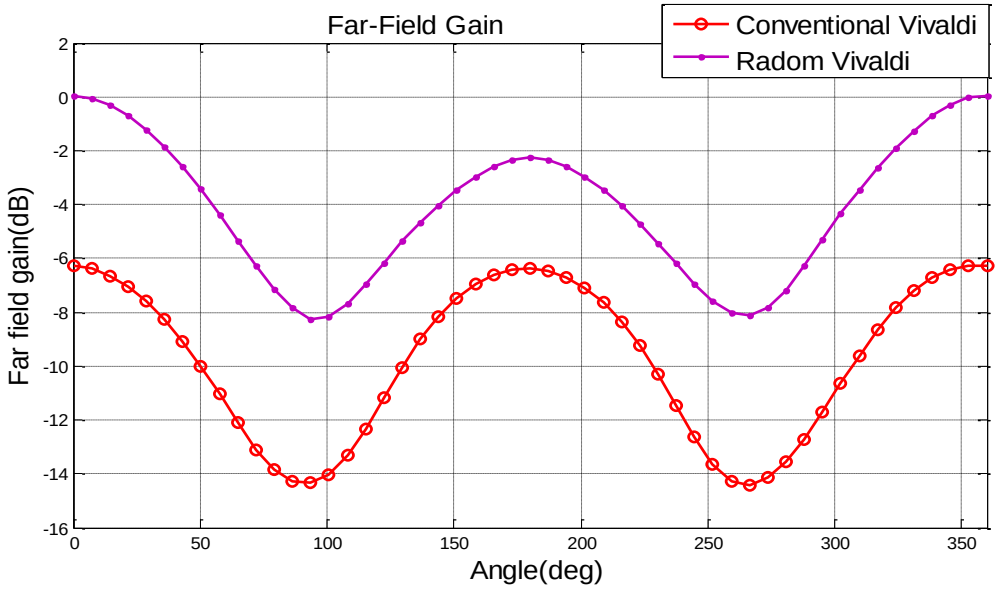

Fig.8.9 Simulated Far Field Gain Plot of Vivaldi Antenna
with and without Radome Boundary.

E_theta and E_phi typically describes the radiated electric field theta and phi components at far field. The electric field components are basically represented in its spherical coordinates. These theta and phi components provide an idea about the collinear and cross polarization behavior of the antenna. From Fig.8.6 and Fig.8.7, it can be observed that the Cross Polarization reduces significantly in case of radome enclosure.

The polarization of the radiated field can be evaluated by the axial ratio. Far field gain value defines the ratio of the power radiated to the total power accepted. From the Fig.8.8, it can be illustrated that the Radome enclosed Vivaldi is more linearly polarized and Fig.8.9, shows that Radome enclosure enhances the performance of Vivaldi antenna to a great extent.

Chapter 9

Conclusion and Future scope

Design, development and fabrication of the patch compensated wideband Vivaldi antenna and its analysis in radome chamber is presented in thesis report. Effects of the problems that are mainly associated with discontinuity at feeding point, fabrication tolerance or associated parasitic capacitance at edges or bent of micro-stripline has been realized during fabrication and testing. These effects introduce the parasitic impedance in antenna design which deteriorates the radiation characteristic of antenna from the simulation result which is realized in terms of S-parameter. A theoretical procedure has been developed for the compensation of the associated problem. Theory explores that the associated effects can be compensated by incorporating the inductive patch on feed line. The developed theory is applied in fabrication and found effective in compensation of the associated problems. In agreement to the desired results, fabricated antenna found providing better gain, wider-beamwidth and low cross polarization. It also provides wider bandwidth as compared to the uncompensated antenna. This theory can be applied without affecting the original design of antenna is the main advantage. After that the design is analyzed in radome chamber. A radome acts as an enclosure around antenna, thereby protecting it from the environment. Moreover, the enclosure results in improved radiation characteristics such as antenna directivity, gain, radiation pattern and polarization and are discussed briefly.

The work can be further enhanced for biomedical as well as radar applications. Integration of metamaterials in the design can be used for medical imaging which works inside the environment of matching liquid for better coupling of power from the antenna to the human tissues. As Vivaldi is the only planner antenna which can work at an X band frequency of range hence it can be effectively incorporated in the applications of radar. Due to its high bandwidth it can also be integrated in mobile communication. However gain of the antenna is not uniform along the entire frequency range of operation. This is still a potential area to work.

References

[1] D.M. Pozar, *Microwave Engineering*, John Wiley & Sons, 1998.

[2] "Approximate Formulas for Line Capacitance and Characteristic Impedance of Microstrip Line," in *IEEE Transactions on Microwave Theory and Techniques*, vol. 29, no. 2, pp. 135-142, Feb 1981.

[3] J. B. Knorr, "Slot-Line Transitions (Short Papers)," in *IEEE Transactions on Microwave Theory and Techniques*, vol. 22, no. 5, pp. 548-554, May 1974.

[4] P. J. Gibson, "The Vivaldi Aerial," *Microwave Conference, 1979. 9th European*, Brighton, UK, 1979, pp. 101-105.

[5] D. Schaubert, E. Kollberg, T. Korzeniowski, T. Thungren, J. Johansson and K. Yngvesson, "Endfire tapered slot antennas on dielectric substrates," in *IEEE Transactions on Antennas and Propagation*, vol. 33, no. 12, pp. 1392-1400, Dec 1985.

[6] E. Gazit, "Improved design of the Vivaldi antenna," in *IEE Proceedings H - Microwaves, Antennas and Propagation*, vol. 135, no. 2, pp. 89-92, April 1988.

[7] B. Shuppert, "Microstrip/slotline transitions: modeling and experimental investigation," in *IEEE Transactions on Microwave Theory and Techniques*, vol. 36, no. 8, pp. 1272-1282, Aug 1988.

[8] J. D. S. Langley, P. S. Hall and P. Newham, "Novel ultrawide-bandwidth Vivaldi antenna with low cross-polarization," in *Electronics Letters*, vol. 29, no. 23, pp. 2004-2005, 11 Nov. 1993.

[9] J. D. S. Langley, P. S. Hall and P. Newham, "Balanced antipodal Vivaldi antenna for wide bandwidth phased arrays," in *IEE Proceedings - Microwaves, Antennas and Propagation*, vol. 143, no. 2, pp. 97-102, Apr 1996.

[10] R. Sloan, M. M. Zinieris, L. E. Davis, "A broadband microstrip to slotline transition," microwave and Optical Technology Letters, Vol. 18, No. 5, August 1998, pp. 339-342.

[11] Joon Shin and D. H. Schaubert, "A parameter study of stripline-fed Vivaldi notch-antenna arrays," in *IEEE Transactions on Antennas and Propagation*, vol. 47, no. 5, pp. 879-886, May 1999.

[12] Tan-Huat Chio and D. H. Schaubert, "Parameter study and design of wide-band widescan dual-polarized tapered slot antenna arrays," in *IEEE Transactions on Antennas and Propagation*, vol. 48, no. 6, pp. 879-886, Jun 2000.

[13] Sang-Gyu Kim and Kai Chang, "A low cross-polarized antipodal Vivaldi antenna array for wideband operation," *Antennas and Propagation Society International Symposium, 2004. IEEE*, 2004, pp. 2269-2272 Vol.3.

[14] K. V. Dotto, M. J. Yedlin, J. Y. Dauvignac, C. Pichot, P. Ratajczak and P. Brachat, "A new non-planar Vivaldi antenna," *2005 IEEE Antennas and Propagation Society International Symposium*, 2005, pp. 565-568 Vol. 1A.

[15] Li Tianming, R. Yuping and N. Zhongxia, "Analysis and Design of UWB Vivaldi Antenna," *Microwave, Antenna, Propagation and EMC Technologies for Wireless Communications, 2007 International Symposium on*, Hangzhou, 2007, pp. 579-581.

[16] P. Cerny and M. Mudroch, "Back radiation minimization of ultra-wideband Vivaldi antenna for radar application," *2009 3rd European Conference on Antennas and Propagation*, Berlin, 2009, pp. 3335-3339.

[17] C. Deng and Y. j. Xie, "Design of Resistive Loading Vivaldi Antenna," in *IEEE Antennas and Wireless Propagation Letters*, vol. 8, no. , pp. 240-243, 2009.

[18] X. Artiga, J. Perruisseau-Carrier, P. Pardo-Carrera, I. Llamas-Garro and Z. Brito-Brito, "Halved Vivaldi Antenna With Reconfigurable Band Rejection," in *IEEE Antennas and Wireless Propagation Letters*, vol. 10, no. , pp. 56-58, 2011.

[19] T. Im and K. Kim, "Beam correction of Vivaldi antenna using shorting pin structure," *Antennas and Propagation (APSURSI), 2011 IEEE International Symposium on*, Spokane, WA, 2011, pp. 620-621.

[20] Song Lizhong and Fang Qingyuan, "Design and measurement of a kind of dual polarized Vivaldi antenna," *Cross Strait Quad-Regional Radio Science and Wireless Technology Conference (CSQRWC), 2011*, Harbin, 2011, pp. 494-497.

[21] A.Zhou and T. J. Cui, "Directivity Enhancement to Vivaldi Antennas Using Compactly Anisotropic Zero-Index Metamaterials," in *IEEE Antennas and Wireless Propagation Letters*, vol. 10, no. , pp. 326-329, 2011.

[22] Y. Wu, J. Lu, Y. Liu and H. Yang, "Modified design of the antipodal Vivaldi antenna," *Antennas, Propagation & EM Theory (ISAPE), 2012 10th International Symposium on*, Xian, 2012, pp. 316-319.

[23] Y. W. Wang, G. M. Wang, X. J. Gao and C. Zhou, "Double-slot Vivaldi antenna with improved gain," in *Electronics Letters*, vol. 49, no. 18, pp. 1119-1121, August 29 2013.

[24] C. Xinyu, Z. Jinling, Y. Hongzhen, Z. Guozhong, L. Hourong and W. Suhua, "Improve open slot Vivaldi antenna design for terahertz," *2014 39th International Conference on Infrared, Millimeter, and Terahertz waves (IRMMW-THz)*, Tucson, AZ, 2014, pp. 1-2.

[25] S. H. He, W. Shan, C. Fan, Z. C. Mo, F. H. Yang and J. H. Chen, "An Improved Vivaldi Antenna for Vehicular Wireless Communication Systems," in *IEEE Antennas and Wireless Propagation Letters*, vol. 13, no. , pp. 1505-1508, 2014.

[26] J. Wu, Z. Zhao, Z. Nie and Q. H. Liu, "A Printed UWB Vivaldi Antenna Using Stepped Connection Structure between Slotline and Tapered Patches," in *IEEE Antennas and Wireless Propagation Letters*, vol. 13, no. , pp. 698-701, 2014.

[27] M. Sonkki, D. Sánchez-Escuderos, V. Hovinen, E. T. Salonen and M. Ferrando-Bataller, "Wideband Dual-Polarized Cross-Shaped Vivaldi Antenna," in *IEEE Transactions on Antennas and Propagation*, vol. 63, no. 6, pp. 2813-2819, June 2015.

[28] I. T. Nassar and T. M. Weller, "A Novel Method for Improving Antipodal Vivaldi Antenna Performance," in *IEEE Transactions on Antennas and Propagation*, vol. 63, no. 7, pp. 3321-3324, July 2015.

[29] A.M. De Oliveira, M. B. Perotoni, S. T. Kofuji and J. F. Justo, "A Palm Tree Antipodal Vivaldi Antenna with Exponential Slot Edge for Improved Radiation Pattern," in *IEEE Antennas and Wireless Propagation Letters*, vol. 14, no. , pp. 1334-1337, 2015.

[30] A. Dastranj, “Wideband antipodal Vivaldi antenna with enhanced radiation parameters,” in *IET Microwaves, Antennas & Propagation*, vol. 9, no. 15, pp. 1755-1760, 12 10 2015.

[31] M. Moosazadeh and S. Kharkovsky, “A Compact High-Gain and Front-to-Back Ratio Elliptically Tapered Antipodal Vivaldi Antenna with Trapezoid-Shaped Dielectric Lens,” in *IEEE Antennas and Wireless Propagation Letters*, vol. 15, no. , pp. 552-555, 2016.

[32] Y. J. Hu, Z. M. Qiu, B. Yang, S. J. Shi and J. J. Yang, “Design of Novel Wideband Circularly Polarized Antenna Based on Vivaldi Antenna Structure,” in *IEEE Antennas and Wireless Propagation Letters*, vol. 14, no. , pp. 1662-1665, 2015.

[33] O. O'Conchubhair, K. Yang, P. McEvoy and M. J. Ammann, “Amorphous Silicon Solar Vivaldi Antenna,” in *IEEE Antennas and Wireless Propagation Letters*, vol. 15, no. , pp. 893-896, 2016.

[34] R. P. Yadav, S. Kumar, and S. V. Kulkarni, “Design and Development of the 3dB patch compensated tandem hybrid coupler,” *Review of Scientific Instruments,* 84, 014702 (2013).

[35] R. P. Yadav, S. Kumar, and S. V. Kulkarni, “Design and development of ultra-wideband 3dB hybrid coupler for ICRF heating in Tokamak,” *Review of Scientific Instruments,* 85, 044706 (2014).

[36] C. Gupta and A. Gopinath, “Equivalent Circuit Capacitance of Microstrip Step Change in Width,” in *IEEE Transactions on Microwave Theory and Techniques*, vol. 25, no. 10, pp. 819-822, Oct 1977.

[37] Roudot, B.; Mosig, J.R.; Gardiol, F.E.; “Radome Effects on Microstrip Antenna Parameters,” 17th European Microwave Conference, 1987. Oct. 1987 Page(s):771 – 777.

[38] H.Jiang, H.Arai, Y.Ebine; “Antenna-radome interaction of 2GHz band 120° beam antenna,” IEEE Antennas and Propagation Society International Symposium, 8-13 July 2001.Vol. 3, Page(s):66-69.

List of Publications

1. Rajveer Dhawan, Gurkirandeep Kaur, "Vivaldi Antenna Simulation on Defining Parameters, Parametric Study and Results," Shannon100, 3rd International Conference on Computing Sciences, April 2016.

2. Rajveer Dhawan, Vinay Kumar, "Radome Based Vivaldi Antenna with Improved Gain and Directivity," communicated to *International Conference on Advanced Computing and Intelligent Engineering (ICACIE).*

3. Rajveer Dhawan, Rana Pratap Yadav, Vinay Kumar, "Design and development of patch compensated wideband Vivaldi antenna," communicated to *IET Microwaves, Antennas & Propagation*.

Rajveer_801463020

by Rajveer Dhawan

FILE	THESIS_REPORT_FINAL_AUTOSAVED.DOCX (1.98M)		
TIME SUBMITTED	12-JUL-2016 05:56PM	WORD COUNT	9830
SUBMISSION ID	689222065	CHARACTER COUNT	54991

Rajveer_801463020

ORIGINALITY REPORT

10%	3%	9%	%
SIMILARITY INDEX	INTERNET SOURCES	PUBLICATIONS	STUDENT PAPERS

PRIMARY SOURCES

1	docslide.us Internet Source	1%
2	De Oliveira, Alexandre M., Marcelo B. Perotoni, Sergio T. Kofuji, and Joao F. Justo. "A Palm Tree Antipodal Vivaldi Antenna With Exponential Slot Edge for Improved Radiation Pattern", IEEE Antennas and Wireless Propagation Letters, 2015. Publication	1%
3	Yong-Jin Hu, Zhi-Mo Qiu, Bo Yang, Shu-Jie Shi, Jian-Jun Yang. "Design of Novel Wideband Circularly Polarized Antenna Based on Vivaldi Antenna Structure", IEEE Antennas and Wireless Propagation Letters, 2015 Publication	1%
4	Kiourti, Asimina, and Konstantina S. Nikita. "Antennas and RF Communication", Handbook of Biomedical Telemetry, 2014. Publication	1%
5	Dutta, Koushik, Debatosh Guha, Chandrakanta Kumar, and Yahia M. M. Antar.	<1%